ANALYTICAL AND EXPERIMENTAL STUDY OF ANNULAR TWO-PHASE FLOW FRICTION PRESSURE DROP UNDER MICROGRAVITY

A Thesis

by

NGOC THANH NGUYEN

Submitted to the Office of Graduate Studies of
Texas A&M University
in partial fulfillment of the requirements for the degree of

MASTER OF SCIENCE

December 2009

Major Subject: Nuclear Engineering

ANALYTICAL AND EXPERIMENTAL STUDY OF ANNULAR TWO-PHASE FLOW FRICTION PRESSURE DROP UNDER MICROGRAVITY

A Thesis

by

NGOC THANH NGUYEN

Submitted to the Office of Graduate Studies of
Texas A&M University
in partial fulfillment of the requirements for the degree of

MASTER OF SCIENCE

Approved by:

Chair of Committee,	Frederick R. Best
Committee Members,	Karen Vierow
	Yassin A. Hassan
Head of Department,	Raymond Juzaitis

December 2009

Major Subject: Nuclear Engineering

ABSTRACT

Analytical and Experimental Study of Annular Two-Phase Flow Friction Pressure Drop under Microgravity. (December 2009)

Ngoc Thanh Nguyen, B.S., Texas A&M University

Chair of Advisory Committee: Dr. Frederick R. Best

Two-phase liquid-gas flow has a wide variety of applications in space, including active thermal control systems, high-power communications satellites, heat pumps and space nuclear reactors. Two-phase systems have many potential advantages over current single-phase systems due to reductions in system size, weight and power consumption. The mechanisms of pressure drop, heat transfer coefficients, void fractions, and flow regimes must be well understood under microgravity conditions in order to design reliable two-phase systems. The main objective of this present research is to develop a new mathematical model that can accurately predict the annular two-phase friction pressure drop to optimize the design of two-phase systems. The two-phase flow tests were conducted aboard the NASA KC-135 aircraft by the Interphase Transport Phenomena (ITP) group from Texas A&M University. The two-phase flow pressure drops were measured across a single transparent test section 12.7 mm ID and 1.63 m long in annular regimes under microgravity conditions during two flight campaigns. Different from previous work, this was the first time both the void fraction and the film thickness were measured under microgravity conditions. The empirical correlations for

the interfacial friction factor and void fraction were developed from 57 experimental data using a linear least squares regression technique. The annular two-phase friction pressure drop can be predicted by the new mathematical model requiring only knowledge of the length and diameter of the tube, liquid and vapor mass flow rates, and properties of the working fluid. In addition, the new mathematical model was validated using Foster-Miller & ITP data collected over twelve flights aboard the KC-135 with working fluid R-12 (77 data points), Sundstrand data collected aboard the KC-135 with working fluid R-114 (43 data points) and Zhao and Rezkallah data aboard the KC-135 with working fluid water and air (43 data points). Compared with the Lockhart-Martinelli model, Wheeler model, Chen model and homogeneous model, the new mathematical model is the optimal model for predicting the two-phase friction pressure drop in annular regimes. The majority of the data falls within +-20% of the proposed correlation and the average error is 12 %.

DEDICATION

To my parents

ACKNOWLEDGEMENTS

First, I would like to express my sincerest gratitude and appreciation to Dr. Frederick R. Best, my advisor at the Texas A&M University, for his guidance, patience and support throughout the course of this research.

Next, I would like to express my special thanks for both seniors in the Interphase Transport Phenomena Laboratory (ITP) group, Dr. Ryoji Oinuma and Dr. Cable Kurwitz. They are shaped and talent engineers who spent a large amount of their time to train me throughout works at ITP lab. I also would like to acknowledge all members of ITP group who worked in two-phase flow under reduced gravity such as Wheeler, Hurlbert, Reinarts, Valota and others. Their pioneer works provided me a solid foundation to complete this thesis.

Finally, I would like to thank my parents, Nguyen Phan Nam and Tran Thi Nguyen Anh, my brother, Nguyen Ngoc Sang, and my wife, Nguyen Thi Minh Nguyet for their encouragement, patience and love.

NOMENCLATURE

A	Cross section area (m^2)
D	Tube inner diameter (m)
DP_{exp}	Experimental pressure drop (Pa)
G	Mass flux ($kg/s.m^2$)
L	Tube length (m)
P	Pressure (Pa)
R_i	Interfacial radius (m)
R_w	Tube radius (m)
Re_f	Liquid phase Reynolds number (dimensionless)
Re_g	Vapor phase Reynolds number (dimensionless)
S	Slip ratio (dimensionless)
We	Weber number (dimensionless)
$\frac{dp}{dx}$	Tube axial pressure gradient (N/m3)
$\frac{du_f}{dx}$	Liquid phase velocity gradient (m/s.m)
f_i	Interfacial friction factor (dimensionless)
f_g	Smooth tube vapor friction factor (dimensionless)
g_x	x-axis acceleration (m/s^2)
g_y	y-axis acceleration (m/s^2)
g_z	z-axis acceleration (m/s^2)

$\dot{m}_f$	Liquid phase mass flow rate (kg/s)
$\dot{m}_g$	Vapor phase mass flow rate (kg/s)
r	Tube radial location (m)
t	Time (sec)
u_i	Interfacial velocity (m/s)
u_f	Liquid phase velocity (m/s)
u_g	Vapor phase velocity (m/s)
x	Mass quality (dimensionless)
ΔP	Pressure drop (Pa)
α	Void fraction (dimensionless)
β	Volumetric fraction (dimensionless)
χ_{tt}	Martinelli parameter (dimensionless)
μ_f	Liquid phase viscosity ($N.s/m^2$)
μ_g	Vapor phase viscosity ($N.s/m^2$)
ρ_f	Liquid phase density (kg/m^3)
ρ_g	Vapor phase density (kg/m^3)
σ	Surface tension (N/m)
τ_w	Wall share stress (N/m^2)
τ_i	Interfacial shear stress (N/m^2)

TABLE OF CONTENTS

Page

CHAPTER

LIST OF FIGURES

Page

LIST OF TABLES

Page

CHAPTER I

INTRODUCTION AND LITERATURE REVIEW

1.1 INTRODUCTION

Vapor-liquid two-phase flows play a vital role in many industrial heat transport processes, engineering applications, and in ordinary life. Two-phase systems have numerous applications in aerospace, chemical and petroleum processes, nuclear reactors, heat-exchangers, and energy transport and energy conversion systems. Due to a wide range of important applications, two-phase flows have been researched actively for several decades. Space applications for two-phase technology are widespread, including thermal control systems, dynamic power systems, space nuclear power systems, life support systems, high-power communications satellites, heat pumps, and the storage and transfer of cryogenic fluids (Hill and Best, 1991)[1]. Due to the increased heat loads anticipated for the NASA Space Station, there are demands for more advanced thermal transport and temperature control techniques (Chen, 1989)[2,3]. Two-phase systems have been chosen as excellent candidates for the design of future space stations. Two-phase flows have many thermal transport advantages over single-phase systems in space power applications. First, since the heat transfer coefficients in two-phase flow with phase

---

This thesis follows the style of *Journal of Thermophysics and Heat Transfer*.

change are higher than that in single-phase flow, smaller two-phase systems can carry as much heat as single-phase systems with much smaller size (Gabriel, 2006)[4]. For instance, a heat exchanger in the two-phase systems has a smaller size with higher heat flux capability than that in single-phase systems.

In addition, the two-phase systems require considerably lower mass flows than do equivalent single phase systems. Thus, the two-phase systems can benefit greatly from reductions in pumping power, system size, and weight.

Since two-phase flows for terrestrial conditions have been studied and researched over several decades, a large amount of data, models, and correlations exists for two-phase flow phenomena for terrestrial applications. However, very little empirical and analytical modeling of two-phase flow have been done under microgravity conditions due to the limited access to the microgravity environment and high costs associated with it. As the result of that, a better understanding the mechanisms and behaviors of two-phase flows in microgravity is a must for the full benefits of using two-phase flow technology in space applications.

The objectives of the present research are:

- To examine the effect of the gravitational acceleration on average film thickness, void fraction and interfacial friction factor.
- To develop empirical correlations for the interfacial friction factor and the void fraction based on experimental data collected by the Interphase Transport Phenomena (ITP) Laboratory at Texas A&M University.

- To examine the effect of the gravitational acceleration on the two-phase flow friction pressure drops in the annular regime, as well as to develop a new mathematical model to predict the annular two-phase flow friction pressure drops under microgravity conditions.

1.2 LITERATURE

Albers and Macosko (1966)[5] conducted an experimental investigation in a converted Navy bomber flying through a portion of a ballistic path to determine the differences between the pressure losses of nonwetting condensing flow of mercury vapor in 1-g and 0-g environments. In general, the experimental system was a single-pass boiling and condensing system consisting of a mercury-expulsion and liquid-flow measuring system, mercury pre-heater, a high flux boiler, a main boiler, a vapor-flow-measuring Venturi, a horizontal condensing tube, and a mercury receiver for collecting the condensed mercury. The local and overall pressure drops were measured for a horizontal, stainless-steel tube that was 87-inch-long and 0.311 inch-ID with six pressure taps located at 1 foot intervals starting 12 inches from the tube inlet. Annular flows were achieved in the experiment. The overall static pressure drops varied from 0.2 to 2.2 psi, while the total pressure loss varied from 1.4 to 5.4 psi. There was a little difference between 1-g and 0-g pressure losses at flow rates of 0.028 and 0.046 lbm/s. The Lockhart-Martinelli correlation predicted the two phase friction multiplier to within 30% and the pressure gradient to within 70% for the high velocity, high quality region of the condensing tube.

The measured pressure gradients both for 1-g and 0-g were greater than the analytical predictions of Lockhart-Martinelli for the low quality region of the tube.

In October 1987, NASS-JSC contracted with Sundstrand to build a two-phase thermal management system which allowed two-phase flow observation and pressure drop measurement in reduced gravity. The test loop was first checked out on the ground at Sundstrand and at NASA-JSC to establish an operating procedure, determine the test loop performance and run flight test simulations. The reduced gravity tests were conducted aboard the NASA-JSC KC135 reduced gravity aircraft on two separate days. The adiabatic test section consisted of two transparent portions; a straight section with a 72-in long (1.83 m) and 0.623-in (1.58 cm) diameter and a curved section with a 180 degree bend. The saturated Refrigerant-114 was pumped to a flow evaporator where two-phase flow with the desired quality was generated and passed to the adiabatic test section. The flow regimes were observed within the transparent test section using high-speed cinematography. During low-G conditions, slug flow was observed over the quality range from 5 to 10% and annular flow existed over a quality range from roughly 15 to 90%. The two-phase pressure drops were measured by the differential pressure transducers with nominal accuracy of +- 0.05 psi. The observed flow qualities ranged from 0.05 to 0.8 and the pressure drops ranged from 0.09 psi at low quality to 0.277 psi at high quality. In addition, the total mass flux was roughly 191 kg/m^2-s at the highest quality and was 230 kg/m^2-s at the lowest quality. A total of fifty-four parabolas were collected during two days of testing. The measured straight section pressure drops was compared to predictive values using a number of two-phase pressure drop models,

including the Heat Transfer Research Institute (HTRI), Lockhart and Martinelli, Friedel, Chisholm B-type, Taitel and Dukler, homogeneous and the annular flow model using the Premoli void fraction correlation over entire range of qualities. It was recommended that the HTRI or Friedel correlations used for predicting pressure drops in the straight section and the Chisholm B and C be used for predicting the pressure drops in curved sections and flow discontinuities. The pressure drops in zero-gravity were reported to be significantly larger than the 1-g pressure drop for the same conditions of mass flux and quality.

Heppner, King and Littles (1975)[6] performed experiments at earth gravity and aboard the KC-135 aircraft flying parabolic trajectories. The tests were performed with air/water in a transparent test section with L/D =20. The test section consisted of a rigid plastic block with a 2.5 inch square cross section. A cylindrical flow passage with a diameter of 1 inch was bored along the length of the block. Water was introduced through four peripheral ports at a location 3 inches from the entrance. The flow regimes were recorded by a high speed camera, and data, including the total flow rate, mass quality and static pressures, were recorded during the 2-g and 0-g accelerations. The measured pressure drops in zero-gravity were reported to be significantly larger in comparison with equivalent conditions tested at 1-g. Based on a series of the observed flow regimes at 1-g and 0-g, it was concluded that the gravity level affects the flow patterns.

During 1900 - 1992, Wheeler, Lambert, Reinarts, Miller, and Best[7,8,9,10,11] completed research on two-phase flow behaviors under microgravity conditions including two-

phase friction pressure drop, two-phase heat transfer coefficient, and flow regimes. The experiment was funded by the U.S. Air Force and conducted by Foster-Miller with the aid of Texas A&M University. Zero gravity data were taken aboard the KC-135 over twelve flights (518 parabolas) and extensive testing was performed in 1-g in the Interphase Transport Phenomena (ITP) Laboratory at Texas A&M University. The working fluid was chosen to be Refrigerant-12 because of its low toxicity, low heat of vaporization, material compatibility properties, and high density at acceptable pressures. The main feature of the experimental package is a two phase pump developed by Foster-Miller Inc. The Foster-Miller two-phase pump can accept a mixture of vapor and liquid with any quality at the inlet, separates the two phases to high purity, and provides a pumping head to both phases. Thus, the quality of the two-phase mixture entering the adiabatic test section can be controlled by adjusting the flow rates. The vapor and liquid mass flow rates were measured directly by venturi vapor flow meters and bearingless liquid flow meters. The experiment contained two adiabatic test sections with 119 L/D's long for the larger ID (10.5 mm) and 266 L/D's long for the smaller ID section (4.6 mm). The flows through the two test sections were in opposite directions. Flow images were recorded near the outlet ends of test sections. The flow regimes consisted of annular flow, frothy flow, churn flow, and slug flow in 0-g. A pair of Foxboro Electronic d/p Cell Transmitters with matched pressure seals was used to obtain the pressure drop measurements for each of the adiabatic test sections for mass flow rates between 0.006 and 0.06 kg/s. The corrected pressure drop measurements were compared with a series of predictive models. Lambert found that the homogeneous, and Beattle and Whalley

models showed good agreement with the pressure drops measured for the slug and bubbly/slug flow conditions. Miller and Wheeler concluded that the Troniewski and Ulbrich and Lockhart-Martinelli/Chisholm models predicted the data most accurately for Earth-normal gravity. It was reported that there were no differences in between 1-g and 0-g frictional pressure drops.

Zhao and Rezkallah (1994)[12, 13] conducted experiments at normal gravity and aboard the NASA KC-135 aircraft. Water and air were used as the working fluids. Water was pumped from the pump/separator unit. The rotational speed of the pump and a set of flow venturis were used to control the water flow rate at accuracy 1%. Air was supplied from a compressed air tank attached to the apparatus. Flow control venturis were used to control and measure the air flow rate. The two phase flow was supplied through a mixer. The test section consists of five parts:

1- A vertical upward observation section (12.7 cm long, 0.9525 cm i.d.)

2- A vertical upward heated test section (36 cm long, 0.92525 cm i.d.)

3- A vertical downward observation section (58.4 cm long, 1.27 cm i.d.)

4- A 90 degree bend observation section (7.65 cm radius, 1.27 cm i.d.)

5- A horizontal observation section (39.4 cm long, 1.27 cm i.d.)

Three pressure gauges were located at 25.7 cm (from the mixer outlet), 30.5 cm and 69 cm (down stream from the bottom transducer) and two pressure gradients were obtained from bottom to top (69.0 cm) and from bottom to middle (30.5 cm). The flow regimes including the bubble flow, slug flow, frothy slug-annular flow, and annular flows were observed under microgravity conditions. It was found that the friction

pressure drops at 0-g were within 1 to 14 % higher than those at 1-g at the same flow conditions. The homogeneous model predicted the experimental pressure drop most accurately while the Chisholm's correlation tended to under-predict the pressure drop and the Friedel's model overestimated the pressure drop on all flow regimes.

1.3 THESIS ORGANIZATION

In the second chapter, the experimental procedures and data collection obtained from experiments flown aboard the NASA KC-135 aircraft by ITP & Creare are presented. The third chapter presents the differences of the annular two-phase flow between microgravity conditions and normal gravity conditions. A series of common pressure drop models are presented: Homogenous model, Wheeler model, the Lockart-Marinelli-Chisholm model, and Annular Flow Model/ Chen Model. The results of the film thickness, void fraction and interfacial friction factor modeling were presented in Chapter IV. The empirical correlations for the interfacial friction factor and void fraction are developed from 57 experimental data using a linear least squares regression technique. The last chapter proposes conclusions to the entire thesis.

CHAPTER II

EXPERIMENTAL DESCRIPTION AND PROCEDURE

2.1 INTRODUCTION

This chapter gives a detailed description of the two-phase flow loop, the general instrumentation used for data collection, and the flight campaigns.

2.2 EXPERIMENTAL PACKAGE

A schematic of the Texas A&M University ITP Laboratory two-phase flow test package used in the current thesis is shown in Figure 2.1. The legend for the schematic is shown in Figure 2.2, and Table 2.1 provides a listing of instruments/sensors present in the test bed.

The two-phase flow test bed is a new version of that used by Miller and Wheeler (1993)[9], Lambert and Reinarts (1992) [10]with major modifications including a reduction of overall line length sizes and a removal of the boiling test section. The working.

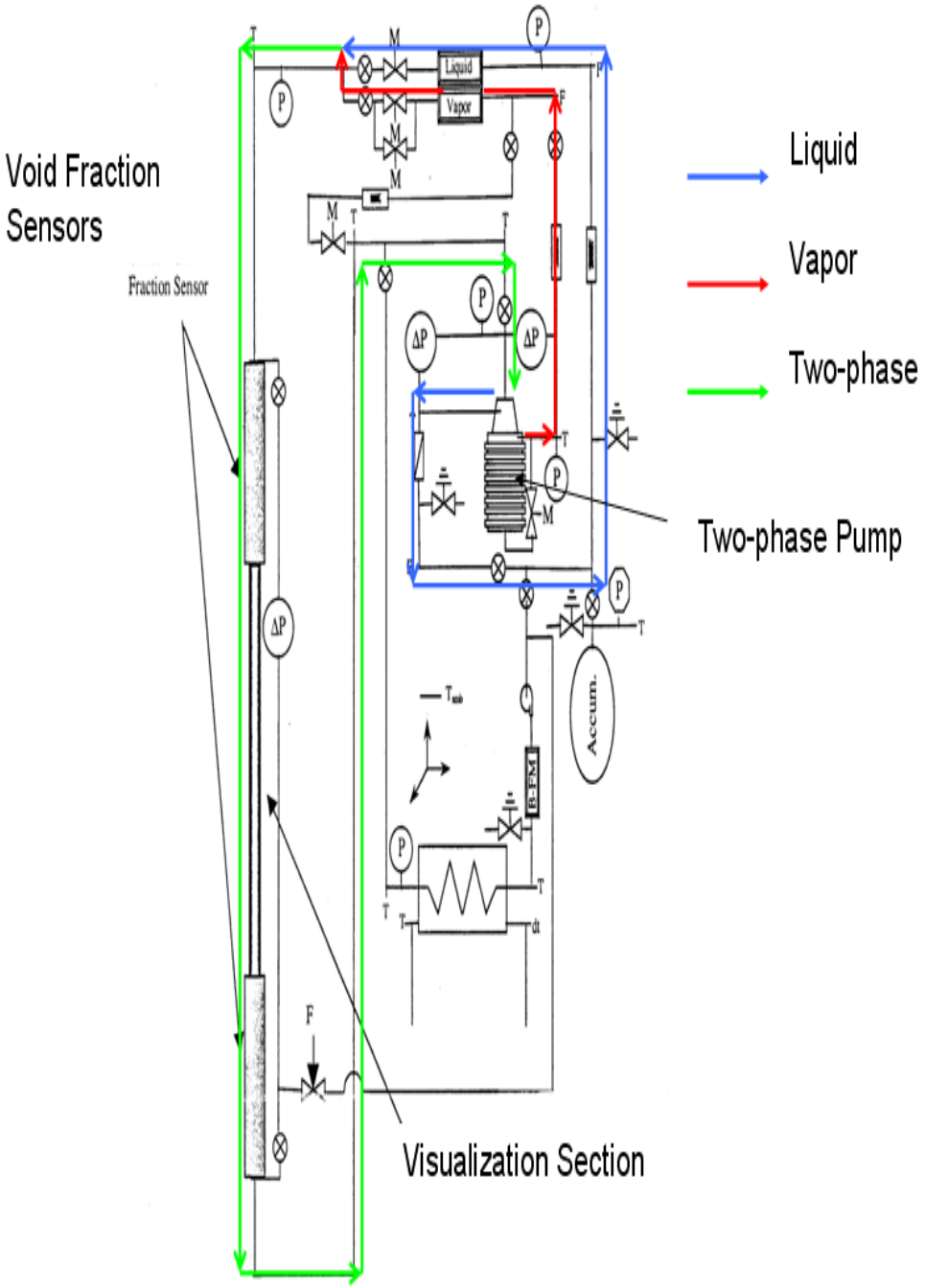

Figure 2.1: Experiment schematic

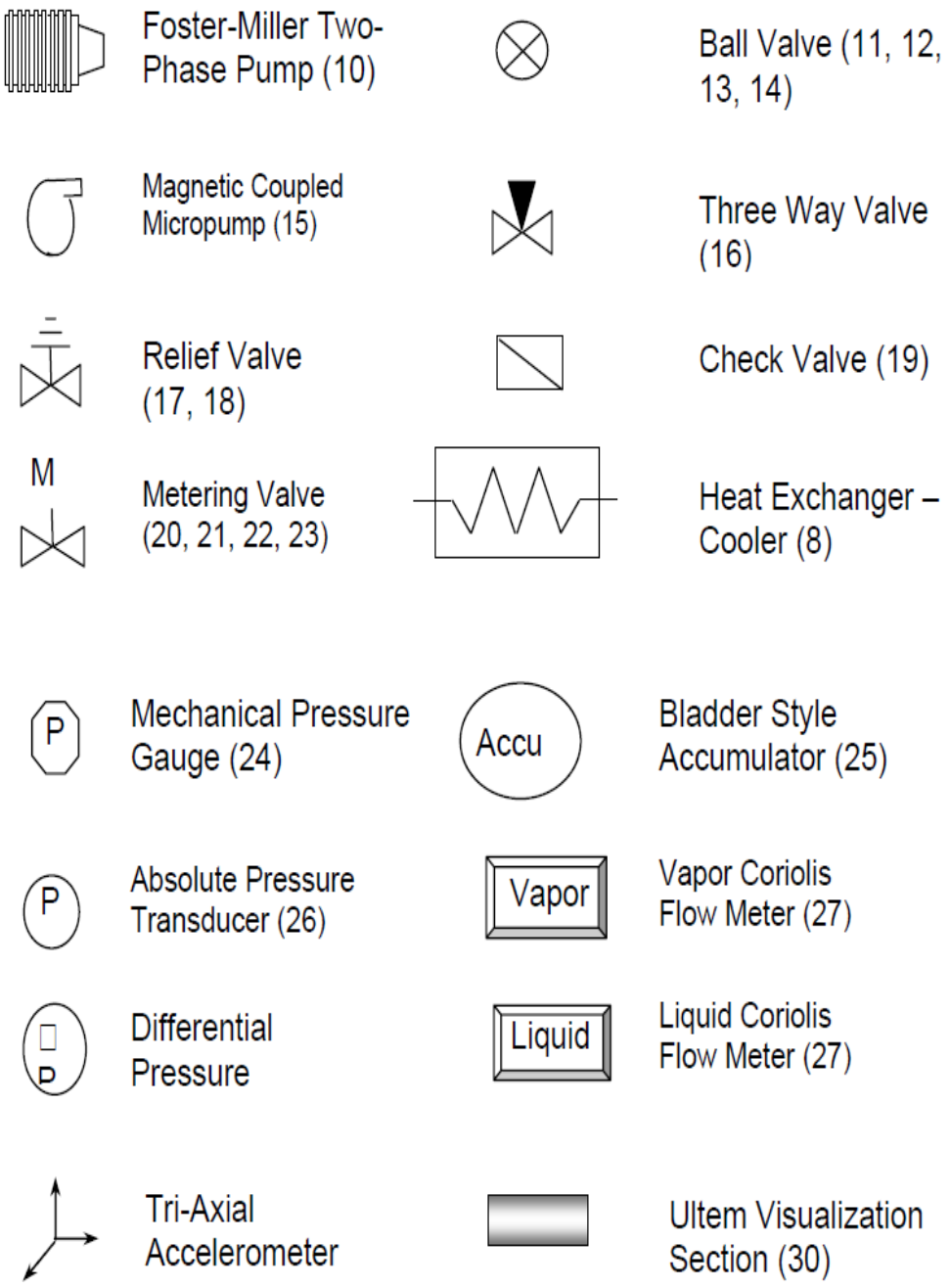

Figure 2.2: Legend

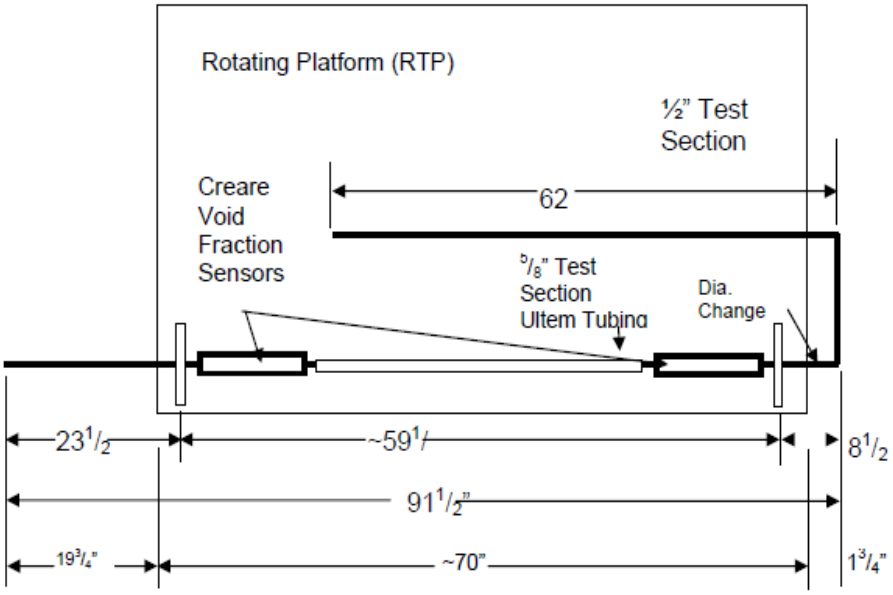

Figure 2.3: Test section schematic

Figure 2.4: Foster Miller package

Table 2.1: Sensor list for the test bed

Sensor #	Sensor Code	Sensor Name	Sensor #	Sensor Code	Sensor Name	Sensor #	Sensor Code	Sensor Name
0	AP1	Pump Vapr Outlet Absolute Pressure	14	TE2	Heat Exchanger R-12 Outlet Temperature	28	GY	Transverse Acceleration
1	AP2	Pump Inlet Absolute Pressure	15	TW1	Heat Exchanger H2O Differential Temperature	29	GZ	Vertical Acceleration
2	AP3	Pump Liquid Outlet Absolute Pressure	16	TWD	Heat Exchanger H2O Differential Temperature	30	VF1-1	Void Fraction Sensor 1 3mm
3	AP4	Heat Exchanger Outlet Absolute Pressure	17	TL1	Pump Liquid Outlet Temperature	31	VF1-2	Void Fraction Sensor 1 6mm
4	AP5	Section 1 Inlet Absolute Pressure	18	TL2	Accumulator Outlet Temperature	32	LD	Micromotion Liquid Density
5	DP1	Pump Vapor Differential Pressure	19	TL3	Micromotion Vapor Temperature	33	VD	Micromotion Vapor Density
6	DP2	Pump Liquid Differential Pressure	20	TV1	Pump Vapor Outlet Temperature	34	VF1-3	Void Fraction Sensor 1 135mm
7	DP3	Section 1 Differential Pressure	21	TV2	Micromotion Vapor Temperature	35	VF2-1	Void Fraction Sensor 2 3mm
8	AP6	Heat Exchanger Inlet Absolute Pressure	22	TA	Ambient Temperature	36	VF2-2	Void Fraction Sensor 2 6mm
9	T1	Section 1 Inlet Temperature	23	ME	Hrat Exchanger R-12 Flowwrate	37	VF2-3	Void Fraction Sensor 2 135mm
10	T2	Section 2 Inlet Temperature	24	MF	Heat Exchanger H2O Flowrate	38	Shear Top	
11	T3	Section 2 Outlet Temperature	25	ML	Micromotion Liquid Mass Flowrate	39	Shear Bottom	
12	T4	Pump Inlet Temperature	26	MV	Micromotion Vapor Mass Flowrate			
13	TE1	Heat Exchanger R-12 Inlet Temperature	27	GX	Axial Acceleration			

fluid is chosen to be dichlorodifluoromethane R-12 because of the following reasons

- Low heat of vaporization results in a wider range of superficial velocities.
- Avoid overheating and possible melt down of the test section.
- Reduce the amount of heat loss to environment because its operating temperature is close to the ambient temperature.
- A larger (ρ_l / ρ_g) results in a wider range of flow variation means a better controlled system.
- Low toxicity, good material compatibility properties, and provides a measureable pressure drop in the adiabatic test section

Compared with air and water at about one atmosphere:

- The R-12 vapor density is about 30 times greater than air.
- The R-12 viscosity is about one-fourth that of water.
- The R-12 surface tension is about a factor of seven smaller than water.

In addition, flow regime transitions occur more at lower vapor velocity with high vapor density, thus tests with refrigerants can identify the flow regimes and the fluid distribution patterns much easier and more clear than tests with air and water.

The facility operated at a temperature and pressure of about 295 K and 600 kPa

The main feature of the experimental package (Figure 2.3 and Figure 2.4) is the two-phase pump designed by Foster-Miller Incorporated. This two-phase pump (Figure 2.5) separates a mixture of vapor and liquid of any quality into single phase constituents and provides a pumping head to both phases. The separation of the phases allows for accurate, direct measurement of the flow rates of each phase, thus

the quality of the two-phase mixture entering the adiabatic test section can be controlled by adjusting the flow rates. In addition, the two-phase pump eliminated the need for subcooling at the pump inlet to prevent damages from cavitation.

Figure 2.5: Foster-Miller two phase pump

Sight glasses in the lines downstream of the pump were used to visually verify the purity of the phases. A hand valve and single-phase pump were installed downstream of the two-phase pump liquid outlet to control the liquid flow to a heat exchanger, which was a copper tube-in-tube type with chilled water from an ice bath on the low temperature or sink-side. A bearingless flow meter was used to measure the flow rate of liquid R-12. The cooled liquid R-12 was then reintroduced to the flow upstream of the two-phase pump inlet. The mass flow rates were measured by Coriolis type flow

meters with an accuracy of +/- 1% for the liquid phase and +/- 2% for the vapor phase. Coriolis flow meters from Figure 2.6 measure mass flow directly by sensing the effect that the flowing fluid has on a vibrating tube (Hurlbert, 2000)[14].

Figure 2.6: Coriolis flow meter

The pressure drop and void fraction measurements were incorporated into a single test section 12.7 mm ID and 1.63 m long. Pressure drop measurements across the adiabatic test section were made via a pair of Foxboro 823 Electronic d/p Cell Transmitters. The transmitters were calibrated over the range of 0 to 12.2 kPa, and had an overall accuracy of +-40 Pa differential. A detailed description of this device can be found in Wheeler (1992)[7] and Reinarts (1991)[15] Two void fraction

instruments designed by Creare Incorporated (Figure 2.7a and Figure 2.7b) were located upstream and downstream in the test section. Each instrument included three sensors, a 3 mm parallel ring sensor, a 6.5 mm parallel ring sensor, and a 135 mm helical sensor. The film thickness in the annular flow regime was measured by the ring sensor, and the volume-averaged void fraction was measured by the helical sensor. The film thickness results from the 6.5 sensors were not used because of their unstable behaviors, (Valota, 2004)[16].

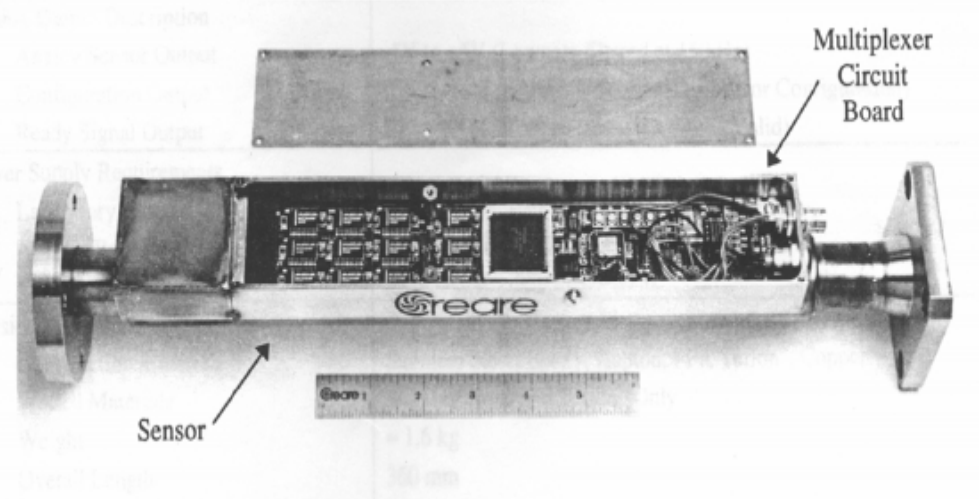

Figure 2.7a: Capacitance void fraction sensors hardware

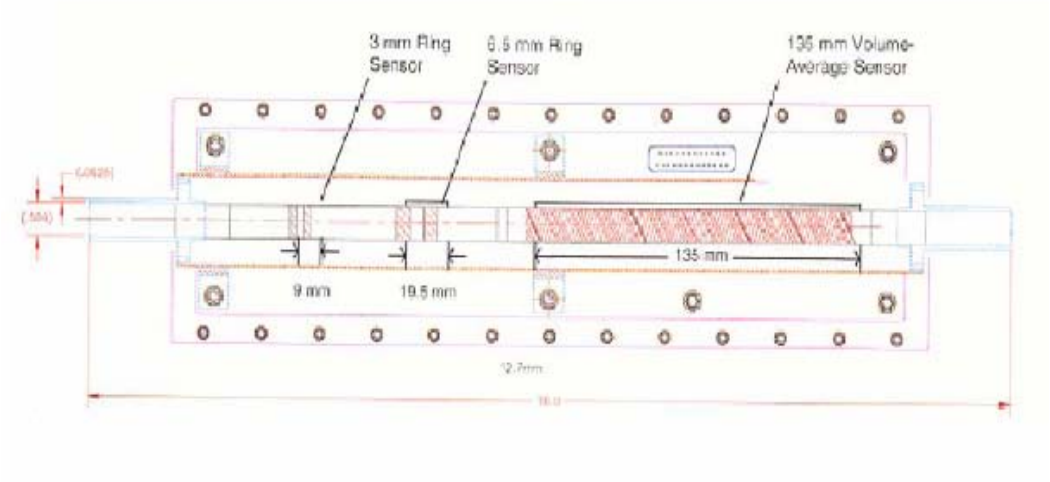

Figure 2.7b: Void fraction sensors in the instrument

Flow visualization and digital imaging of the flow patterns and distribution were possible in the transparent plastic (Ultem) tubing provided by NASA Glenn Research Center.

2.3 FLIGHT PROCEDURE

The experiment was conducted aboard the NASA-Johnson Space Center (JSC) KC-135 aircraft stationed at Ellington Field in Houston, Texas (Figure 2.8). The KC-135 aircraft simulated zero-g or partial-g conditions by flying parabolic trajectories (Figure 2.9).

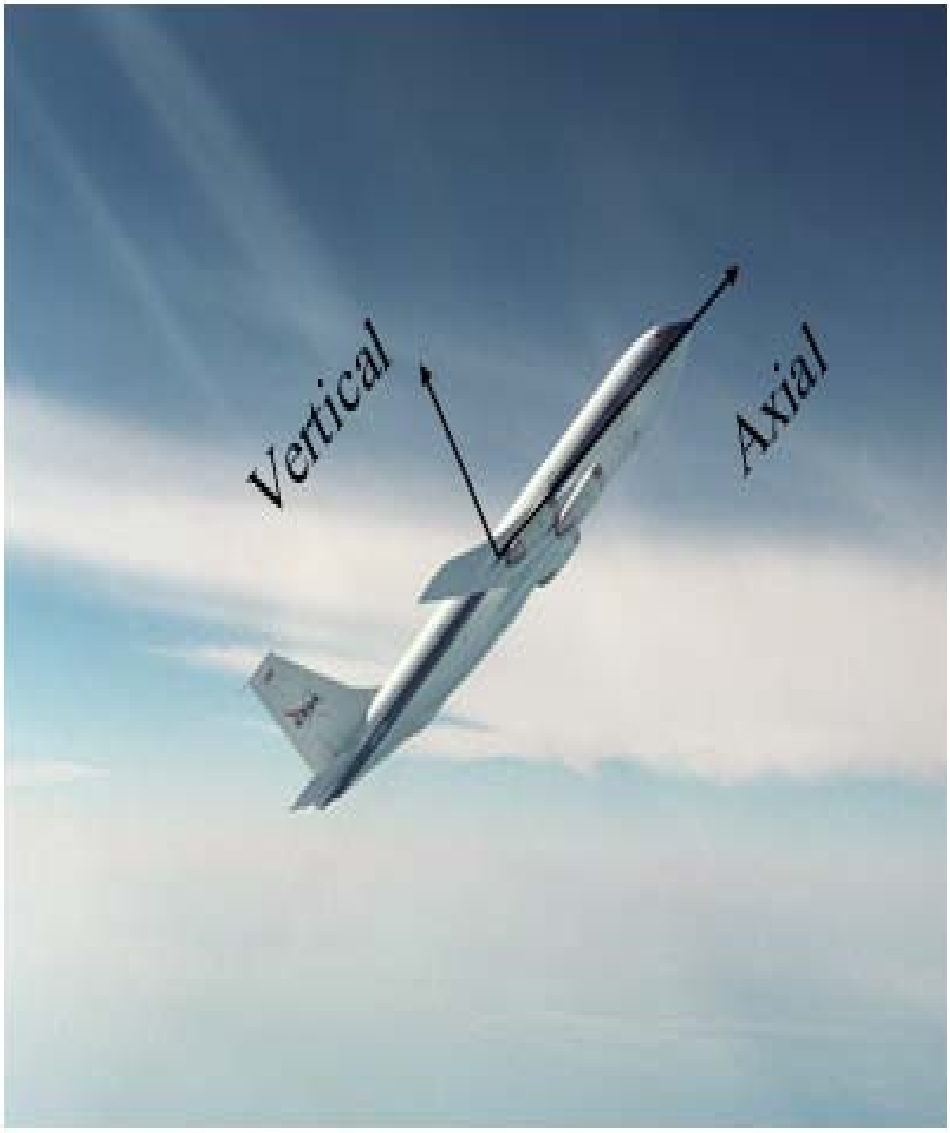

Figure 2.8: NASA’s KC-135 Aircraft

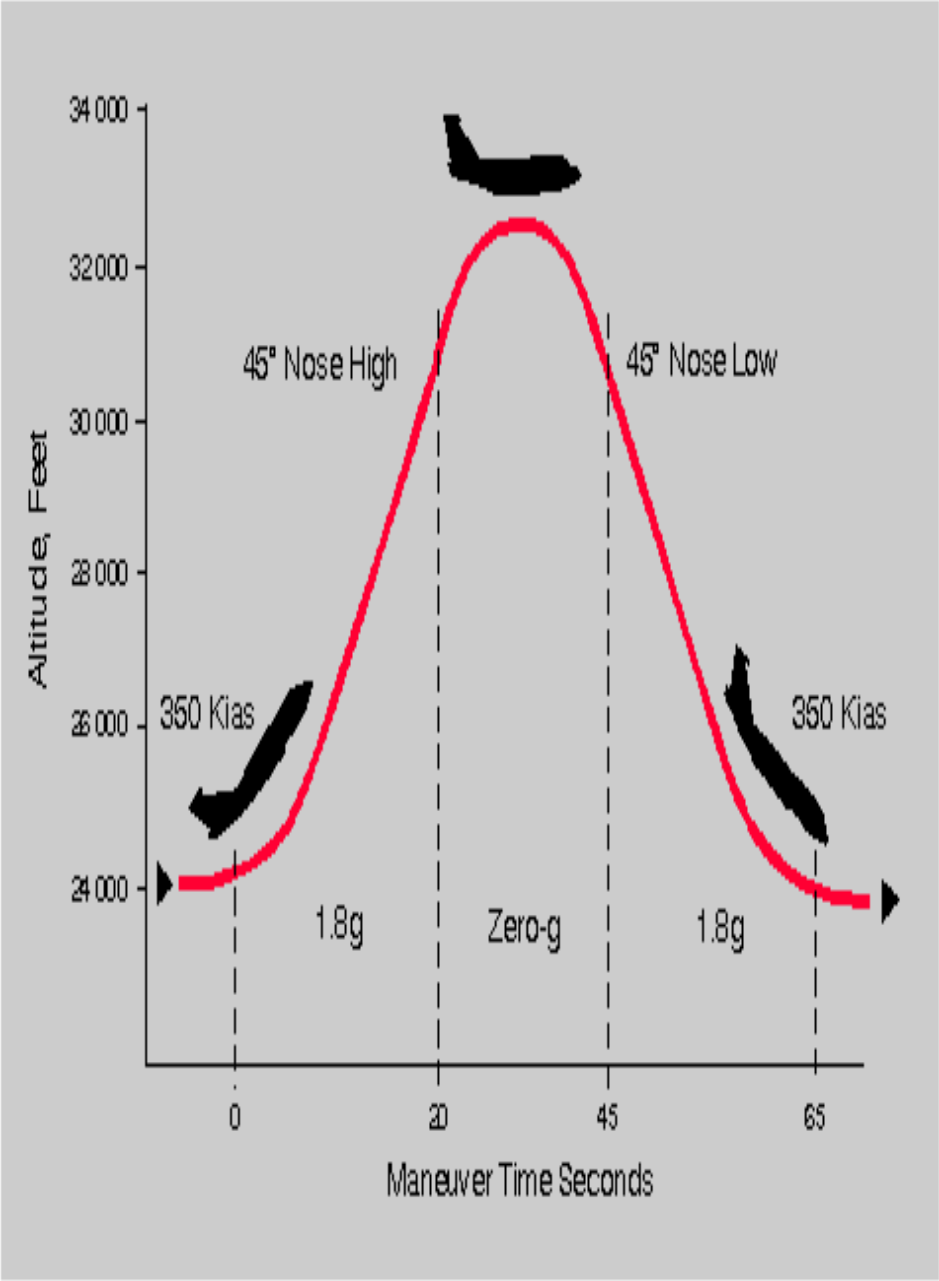

Figure 2.9: KC-135 Flight parabola trajectory

A typical parabolic maneuver includes a 45 degree climb at approximately 1.8-g, followed by a “nose-over” at the top of the parabola where the targeted conditions

are experienced, and then continuation into a 45 degree dive through a 1.8 pullout (Hurlbert, 2000). The reduced gravity period is approximately 20 to 30 seconds during each parabolic maneuver, and a typical flight campaign consists of one week of flying during which more than 40 parabolas are flown in a day. In addition, the airplane is capable of producing lunar (~1/6 g) and Martian (~1/3 g), however this study is based upon data collected in reduced gravity which is a few hundredths of a g.

The experiment was conducted under a very challenging test environment including the size of the cargo door, the interior width of the aircraft cabin, the variation of cabin temperature over a wide range depending on the outside environment, and the short time duration of the reduced gravity periods. Besides the constraints from the test environment, there are operational issues as well. For instances, the weather, the pilot's skills, the aircraft equipment and the response of test equipment/instruments to the variable gravity field were uncontrollable variables that reduced the accuracy and consistency of the experiment. Another important issue is the well-being and performance of the test crew. In previous experiments aboard the NASA KC-135, people experienced mild to severe motion sickness systems during the flights (Hurlbert, 2000)[14].

2.4 EXPERIMENTAL DATA

The flight data used in this thesis was obtained in microgravity flight #4 and flight #5 at 0.01 g acceleration level. Flights #4 and #5 produced excellent data under microgravity conditions with symmetrical flow patterns. The total number of data points collected from flight #4 (60 points) and flight #5 (22 points) was 82 data points. The superficial gas velocity was up to 4 m/s, corresponding to a maximum vapor mass flow rate of 15 g/s. The superficial liquid velocity was up to 0.3 m/s, corresponding to a maximum liquid mass flow rate of 50 g/s. The phase flow rates, pressure drop, void fraction, and acceleration data, along with selected pressure and temperature date, were recorded on a computer at 100 Hz. This frequency allowed recording detailed characteristics of waves in the annular flow regime for over 100 test conditions. Typical results from the experiments are illustrated in Figure 2.10. The figure shows one low-gravity parabola of 20 seconds. The results were averaged over the low-gravity period. The tests were grouped by liquid flow rate and arranged in order of decreasing vapor flow rate within each group. Some of the features observed from the experimental data (Creare Final Report, 2001)[17]:

- Excellent agreement between the film thickness and void fraction measurements at the upstream and downstream locations in the test section.
- The average film thickness (0.5 mm) and the height of fluctuations (0.4 - 1.0 mm) become distinctly larger with decreasing vapor flow rate.
- The frictional pressure drop increases with increasing liquid and vapor flow rate.

- Consistent with the low velocities, droplet entrainment was not observed in the annular flow regime.

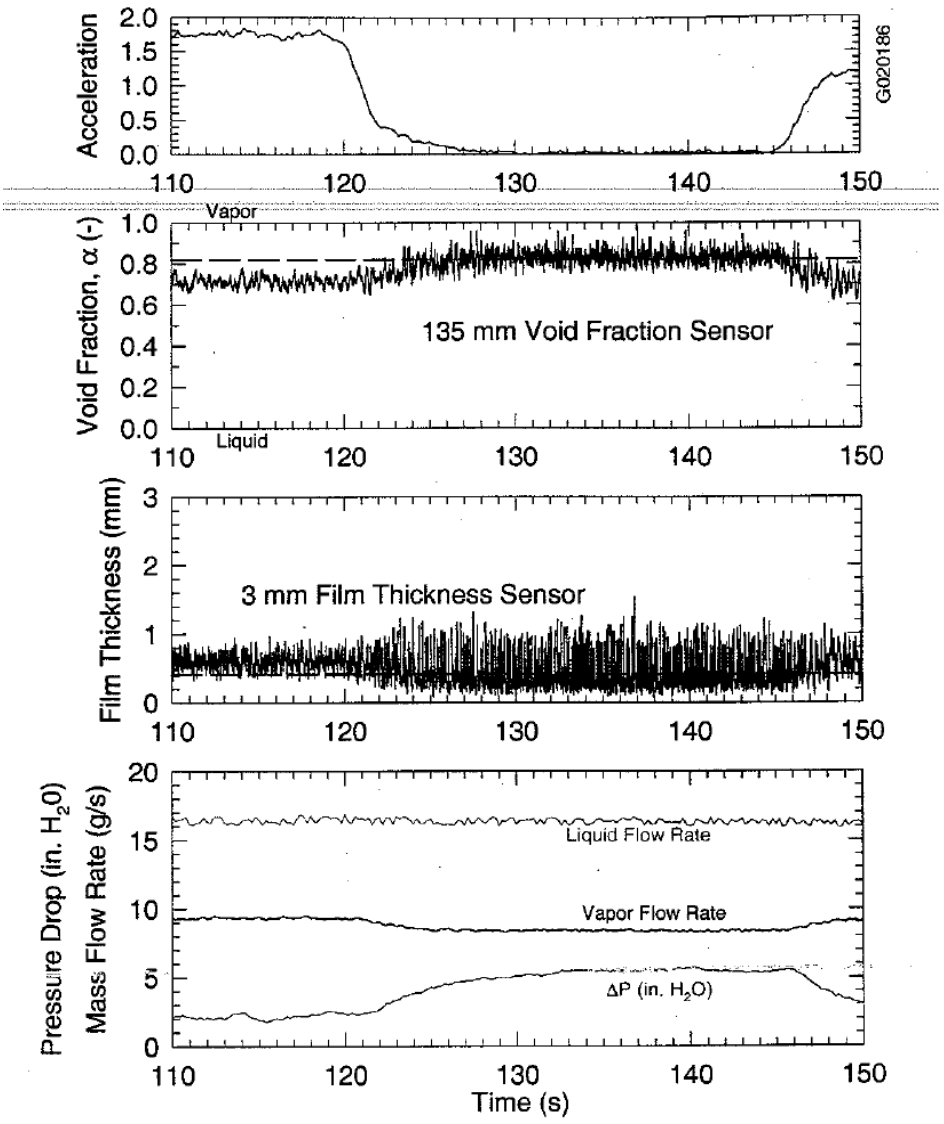

Figure 2.10: Typical results during variation of acceleration in parabolic arc

2.5 CHAPTER SUMMARY

A general overview of the experiment package and experimental methods was presented in this chapter. The experiment environment was described together with the difficulties associated with this environment. Devices to measure void fraction, film thickness, and pressure drop were described.

CHAPTER III

PREVIOUS PRESSURE DROP MODELS

3.1 INTRODUCTION

This chapter describes the previous drop prediction models available in the literature. The physics of annular two-phase flow is presented in microgravity and normal gravity.

3.2 ANNULAR FLOW IN 1-G AND 0-G

A typical annular flow is illustrated in Figure 3.1 a. In the annular flow regime, the liquid flows along the tube wall as a film uniformly distributed around the circumference, while the vapor phase flows along the center of the tube and forms a continuous vapor core. When the vapor flow velocity is high, the interface between the liquid film and the vapor core becomes Helmholtz unstable or highly dynamic and constantly changing leading to the formation of waves at the interface. At low liquid flow rates, the surface is smooth and appears to be laminar between these waves. At high liquid flow rates, disturbance waves appear on the film and the surface is rough and is expected to induce a larger pressure drop than a smooth surface. In addition to the rough interface condition, a fraction of liquid may be entrained in the form of droplets in the vapor core because of the vapor shearing off the disturbance waves. This entrainment of liquid can cause a momentum transfer that can affect the velocity profile, pressure drop, film thickness and heat transfer.

However, the pressure drop model presented in this study does not include any deposition or entrainment.

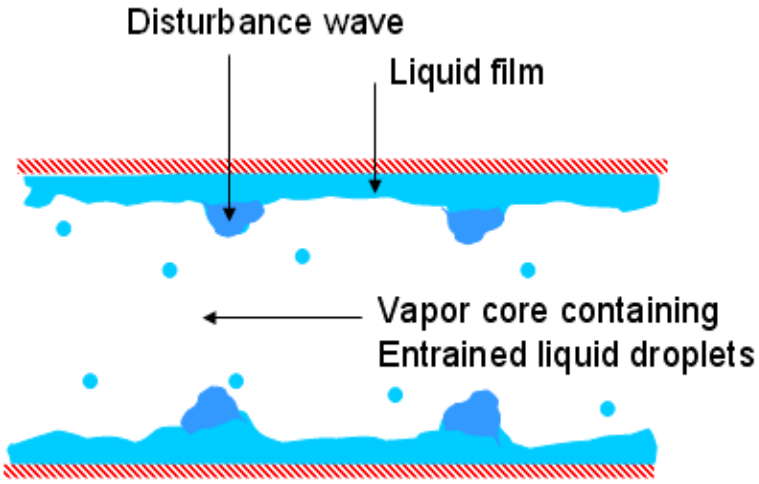

Figure 3.1a: A typical annular flow in 1-g

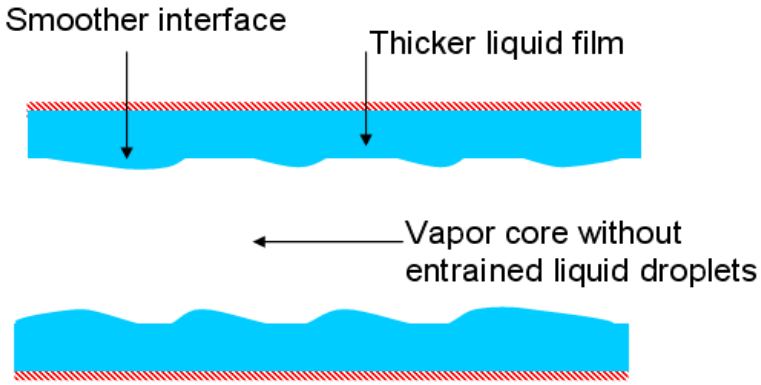

Figure 3.1b: A typical annular flow in 0-g

The forces acting in two-phase flow include pressure gradient, body force, interphase viscous interaction, interphase surface tension effects and external viscous or wall shear stress (Figure 3.1b).

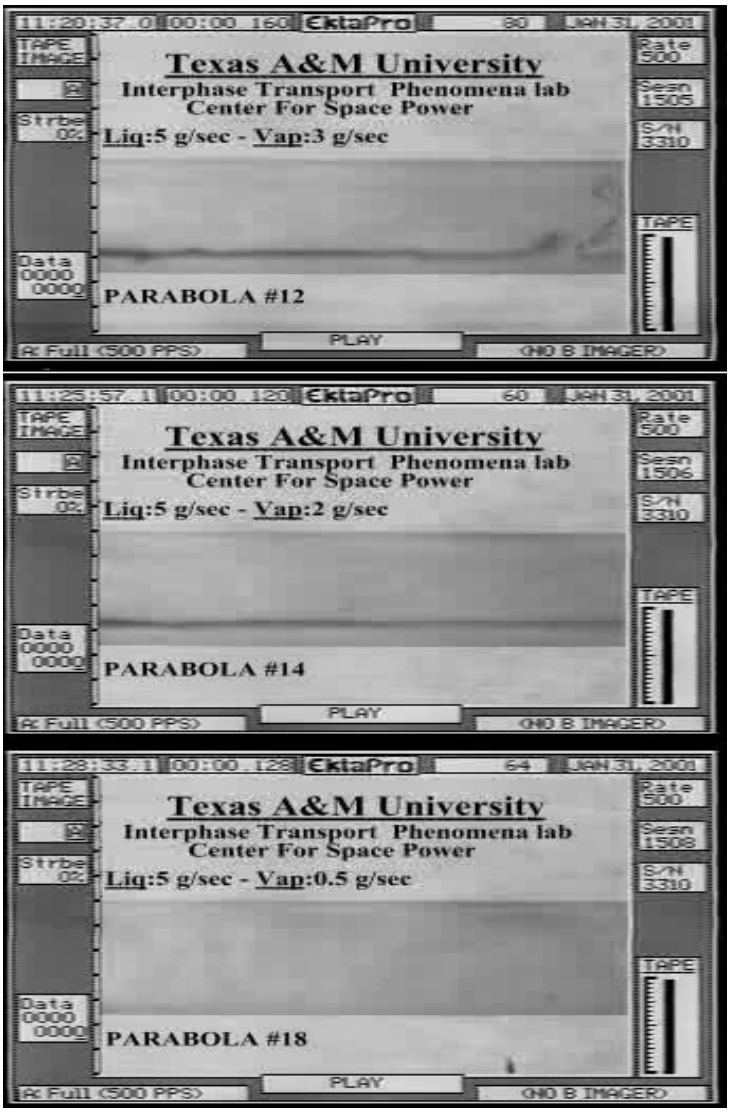

Figure 3.2: A typical annular flow in 0g with decreasing vapor flow rate

The liquid mass flow rate is kept constant at 5 g/s while decreasing the vapor flow rate from 3 g/s to 0.5 g/s. We observed from Figure 3.2 that the average film thickness and the height of fluctuations became distinctly larger.

3.3 ANNULAR PRESSURE DROP AND LIQUID FILM THICKNESS IN A MICROGRAVITY ENVIRONMENT

Reduced gravity experiments are conducted aboard a plane which flies a parabolic flight to simulate a microgravity environment. Bubbly flow, slug flow and annular flow are three major flow regimes observed during the microgravity duration of 20-30 seconds. However annular flow dominates through a wide range of qualities and flow rates (Georgevich, 1991)[18]. For the operation of two phase flow systems, annular flow is preferred while slug flow is usually avoided because of its oscillations. The strong effects of gravity on vapor-liquid phase flow are eliminated under microgravity conditions. These effects are extremely difficult to distinguish and cause a variety of perturbations, instabilities, and undesirable features. Thus, the study of two-phase flow in the absence of gravity effects provides a better understanding of two-phase flow.

Knowledge of the effect of the gravitational acceleration on two-phase flow friction pressure drops in annular regimes is incomplete and is often contradictory among researchers. Rezkallah (1994) explained that buoyancy force is significantly reduced in microgravity conditions and the slip ratio between the two phases is therefore decreased. This leads to a lower liquid-phase fraction in the tube. In this case, the liquid phase flowing in the reduced flow area is accelerated, and the velocity gradient becomes larger near the wall. This would cause the pressure drop to increase. Rezkallah (1994) reported that the microgravity pressure drop was approximately 20% higher than the normal gravity data. Chen (1991) concluded that the pressure drop is strongly affected by the flow regimes for two-phase flow inside tubes and the pressure drop occurring in two-

phase flow under reduced-gravity conditions is two times larger than that for 1-g conditions for the same property conditions and mass flux. Chen (1991) explained that the difference in pressure drops can be due to the difference in the flow regimes. He observed that the microgravity data were mostly annular, while the normal gravity data (horizontal flow) were wavy-stratified and slug. Heppner (1975) also reported a higher pressure drop in microgravity compared to normal gravity for horizontal flow. However, this is opposite to the work of Sridar (1992), who concluded that the frictional pressure drop in microgravity was lower than that for normal gravity and the work of Lambert, Reinarts, Best and Hill (1991), who reported no differences between pressure drops in 0-g and 1-g.

Fukano and Furukawa (1998)[19] conducted a vertical upwards flow experiment using air-water and air-glycerin solutions in 19 mm and 26 mm inner diameter tubes. They reported a thinner film thickness due to a reduction in gravity. De Jong (1999)[20] performed a dimensional analysis on microgravity annular flow data and concluded that a reduction in gravity resulted in a thinner film. He explained that without the influence of gravity, the liquid film is subjected to less body forces, and therefore has a higher average velocity. Based on the conservation of mass, a higher velocity causes a decrease in the flow area, which means a thinner mean film thickness. Fujii (1998) conducted his experiment in a vertical transparent acrylic tube of 10.5 mm I.D and 200 mm length, using a mixture of gaseous nitrogen and water as the working fluid. However, he reported that the mean film thickness was two to five times larger in microgravity than that at normal gravity based on drop tower experiments. Rezkallah (1990), reporting on

the work of Hill (1987)[21], stated that the microgravity annular liquid film flow is thicker when compared to ground tests by approximately two-to-one.

Some of the features that make annular flow in a microgravity environment simpler than at normal gravity are (MacGillivray, 2004)[22]:

1. Around the tube circumference in microgravity annular flow, the waves are not of uniform shape or amplitude; however, the mean film thickness values are azimuthally uniform. Therefore the flow can be considered axisymmetric (Bousman, 1995).
2. Flow reversals due to the gas phase not maintaining sufficient energy to drive the liquid upwards against the gravitational pull do not exist under microgravity conditions.
3. In microgravity, the average microgravity film thickness values are between two and four times larger than those at normal gravity, therefore more accurate measurements of the film can be made.
4. The total pressure drop in two-phase flow can be expressed as the sum of frictional pressure drop, gravitational pressure drop and accelerational pressure drop. Under microgravity conditions, the pressure drops due to acceleration and gravity are significantly reduced, thus the measured pressure drop is only due to friction.

3.4 PREVIOUS PRESSURE DROP MODELS

3.4.1 Homogeneous model

The homogeneous model is the simplest model used for two-phase pressure drop under microgravity. The basic assumption of this model is that the two phases are well mixed and the velocities of the two phases are equal. The mixture density is given by

$$\frac{1}{\rho_m} = \frac{x}{\rho_g} + \frac{1-x}{\rho_l} \tag{3.1}$$

The mixture viscosity given by

$$\mu_m = \mu_g \frac{x\rho_m}{\rho_g} + \mu_m \frac{(1-x)\rho_m}{\rho_l} \tag{3.2}$$

α_m is the homogeneous void fraction given by:

$$\alpha_m = \frac{\rho_l x}{\rho_l x + \rho_g (1-x)} \tag{3.3}$$

The friction factor f_m is calculated from the Blasius equation $f_m = 0.079\,\mathrm{Re}_m^{-1/4}$, in which the Reynolds number is given by $\mathrm{Re}_m = \frac{GD}{\mu_m}$

Thus, the pressure drop can be obtained from

$$\Delta P = \frac{2 f_m G^2 L}{\rho_m D} \tag{3.4}$$

3.4.2 Wheeler's model

Since neither void fraction nor film thickness was measured, Wheeler had to develop his model using a momentum balance between the two phases assuming a smooth interface. The liquid film thickness was determined through a mass flow balance on liquid and gas elements coupling with computer iteration techniques as shown:

For laminar liquid film:

$$\dot{m}_l = -\frac{\pi\rho_l}{8\mu_l}\left(R_i^{\,2} - R_w^{\,2}\right)\frac{dp}{dx} + -\frac{\pi\rho_l}{8\mu_l}g_x\left[\rho_l\left(R_i^{\,2} - R_w^{\,2}\right) + \left(\rho_l - \rho_v\right)R_i^{\,2}\left\{4R_i^{\,2}\left(\frac{1}{2} + \ln\left(\frac{R_w}{R_i}\right)\right) - 2R_w^{\,2}\right\}\right] \tag{3.5}$$

For turbulent liquid film:

$$\dot{m}_1^* = 2\pi\left\{-\frac{\left(\delta^*\right)^2}{\mathrm{Re}^*}\left(1.25\ln\left(\delta^*\right) + 2.125\right) + 3\delta^* + 2.5\ln\left(\frac{\delta^*}{30}\right) + \frac{952.36781}{\mathrm{Re}^*} - 269.7912\right\} \tag{3.6}$$

Or

$$\dot{m}_1^* = 2\pi(8.74)\left[\frac{7}{8}\left(\delta^*\right)^{8/7} - \frac{7}{15}\frac{\left(\delta^*\right)^{15/7}}{\mathrm{Re}^*}\right] \tag{3.7}$$

It is possible to calculate the film thickness from these equations with measured liquid mass flow rate, the g_x acceleration and the pressure gradient, but it is very computer intensive.

Using linear fitting to the calculated film thickness, Wheeler correlated his film thickness as a function of the Martinelli parameter and the two-phase Reynolds number

$$\frac{\delta}{D} \approx CX_{tt}^{\,a}\,\mathrm{Re}_{2\Phi}^{\,b} \approx 3.238X_{tt}^{\,0.4935}\,\mathrm{Re}_{2\Phi}^{\,-0.3535} \tag{3.8}$$

where the Martinelli parameter and the two-phase Reynolds number are defined as

$$X_{tt} = \sqrt{\frac{\Delta P_l}{\Delta P_g}} = \frac{\dot{m}_l}{\dot{m}_g}\sqrt{\frac{\rho_l}{\rho_g}} \tag{3.9}$$

$$Re_{2\Phi} = \frac{GD}{\bar{\mu}} \quad \text{where} \quad \frac{1}{\bar{\mu}} = \frac{x}{\mu_l} + \frac{1-x}{\mu_g} \tag{3.10}$$

By simple algebra for the smooth interface, the relationship between void fraction and film thickness is

$$\alpha = \left(1 - 2\frac{\delta}{D}\right)^2 \tag{3.11}$$

The slip is given by the standard relationship as

$$\bar{S} = \left(\frac{x}{1-x}\right)\left(\frac{\rho_l}{\rho_g}\right)\left(\frac{1-\alpha}{\alpha}\right) \tag{3.12}$$

The interfacial friction factor was correlated based on the momentum balance between the two phases and the measured pressure drop, giving

$$f_i = 0.0032 + 0.076\sqrt{\alpha}\left(\frac{\rho_l}{\rho_g}\right)\left(\frac{1}{S^2}\right)Re_l^{-0.25} \tag{3.13}$$

Whereas the total pressure drop was predicted by:

$$\Delta P = \left(\frac{2 f_i L}{D}\right)\left(\frac{G^2 x^2}{\rho_g \alpha^{2.5}}\right) \tag{3.14}$$

In general, Wheeler's model is more complicated than other models; however, it is reliable because his equations are derived based on the momentum and mass balance on liquid and vapor elements. The complexity of the Wheeler model can be significantly reduced with the benefits of film thickness and void fraction measurements.

3.4.3 Annular Flow Model /Chen Model

The annular flow model is a simple model that could be most suitable for microgravity two-phase flow in annular regimes. The basic assumption of this model is that the two-phase flow is an annular flow with no entrainment and a “smooth” interface. The interfacial shear stress depends on the difference between the vapor velocity and some characteristic interface velocity.

$$\tau_{\mathrm{i}} = \frac{1}{2} f_i \rho_g \left(u_g - u_i\right)^2 \tag{3.15}$$

The interfacial velocity is very small compared to the vapor velocity and assumed to be negligible, then

$$\tau_i = f_i \frac{1}{2} \rho_g u_g{}^2 = f_i \frac{1}{2} \frac{\rho_g j_g{}^2}{\alpha^2} \tag{3.16}$$

The wall shear stress is presented in term of a wall friction factor as

$$\tau_w = f_w \frac{1}{2} \rho_l u_l^2 = f_w \frac{1}{2} \frac{\rho_l j_l^2}{(1-\alpha)^2} \tag{3.17}$$

The pressure gradient at the interface is determined by using the momentum equation neglecting acceleration and gravity terms

$$-\frac{dP}{dz} = \frac{4\tau_i}{D\sqrt{\alpha}} \tag{3.18}$$

Again, the pressure gradient at the wall is determined by using the momentum equation neglecting acceleration and gravity terms at the wall

$$-\frac{dP}{dz} = \frac{4\tau_w}{D} \tag{3.19}$$

The pressure gradient in Equation 3.18 and Equation 3.19 is equated to give

$$\frac{\tau_{\mathrm{i}}}{\tau_w} = \sqrt{\alpha} \tag{3.20}$$

Substituting Equation 3.16, Equation 3.17 into Equation 3.20 leads to

$$\frac{\alpha^{2.5}}{(1-\alpha)^2} = \left(\frac{f_i}{f_w}\right)\left(\frac{\rho_g}{\rho_l}\right)\left(\frac{j_g}{j_l}\right)^2 \tag{3.21}$$

Integrate Equation 3.19 over the length of the actual pipe

$$\int_{P_I}^{P_O} -\mathrm{dP} = \int_0^L \frac{4\tau_{\mathrm{i}}}{D\alpha^{1/2}}dz = \int_0^L 2\mathrm{f}_{\mathrm{i}}\frac{\rho_{\mathrm{g}} j_g^{\ 2}}{D\alpha^{3/2}}dz \tag{3.22}$$

The total pressure drop is determined

$$\Delta P = \left(\frac{2 f_i L}{D}\right)\left(\frac{\rho_g j_g^{\ 2}}{\alpha^{2.5}}\right) \tag{3.23}$$

In order to predict the pressure drop, one can either provide the void fraction to calculate the interfacial friction factor or provide the interfacial friction factor to calculate the void fraction at any given flow conditions**.**

Using reduced gravity data from the flight experiment, Chen made his empirical correlation for the interfacial friction factor

$$f_i = f_g\left\{1+11.7(\delta/D)^{0.39}\right\} \tag{3.24}$$

The void fraction can be written as a function of the slip ratio which is the ratio of vapor velocity and liquid velocity

$$\alpha = \frac{\left(\frac{x}{1-x}\right)\left(\frac{\rho_l}{\rho_g}\right)}{\overline{S}+\left(\frac{x}{1-x}\right)\left(\frac{\rho_l}{\rho_g}\right)} \tag{3.25}$$

The Premoli algorithm is used to determine the slip ratio because this correlation covers a wide range of data and accounts for the mass flux effects

$$\bar{S} = \frac{\bar{u}_g}{\bar{u}_l} = 1 + E_1 \sqrt{\frac{y}{1 + yE_2} - yE_2} \tag{3.26}$$

where

$$\mathrm{y} = \frac{\beta}{1 - \beta}, \mathrm{We} = \frac{\mathrm{G}^2 D}{\sigma \mu_l}, \mathrm{Re}_l = \frac{GD}{\mu_l}$$

$$E_1 = 1.578\,\mathrm{Re}_l^{-0.19} \left(\frac{\rho_l}{\rho_g} \right)^{0.22}$$

$$E_2 = 0.0273 We\,\mathrm{Re}_l^{-0.51} \left(\frac{\rho_l}{\rho_g} \right)^{-0.08}$$

3.4.4 Lockhart and Martinelli/ Chisholm Model

The Lockhart-Martinelli/ Chisholm model is one of the oldest and most widely used techniques for calculating two-phase pressure drops. The two-phase pressure drop is the multiple of the single-phase pressure drop calculated for liquid flowing alone through the tube or vapor phase alone in the tube.

$$\frac{dP}{dz} = \Phi_l^2 \left(\frac{dP}{dz} \right)_l \tag{3.27}$$

The multiplier for liquid flow only through the tubes is given by:

$$\Phi_l^2 = \frac{(dP/dz)_{2\phi}}{(dP/dz)_l} = \left[1 + \frac{20}{X_{tt}} + \frac{1}{X_{tt}^2} \right] \tag{3.28}$$

where $X_{tt} = \left(\frac{\rho_g}{\rho_l}\right)^{0.5} \left(\frac{\mu_g}{\mu_l}\right)^{0.125} \left(\frac{1-x}{x}\right)^{0.875}$, defined as the Martinelli parameter assuming both vapor and liquid phase are in the turbulent flow regimes.

The single-phase frictional pressure gradient is calculated from the Darcy-Weisbach equation:

$$\left(\frac{dP}{dz}\right)_l = -\frac{1}{2} f_l \frac{G^2(1-x)^2}{\rho_l D} \tag{3.29}$$

where the liquid friction factor is given by:

$$f_l = 0.316\left(\frac{G(1-x)D}{\mu_l}\right)^{-0.25} \tag{3.30}$$

Although this correlation is simple, it is not very accurate. Bousman (1995) reported that the Lockart-Marinelli-Chisholm model can predict the annular flow pressure drop with about +- 20 % accuracy.

3.5 CHAPTER SUMMARY

This chapter presented the differences of the annular two-phase flow between microgravity conditions and normal gravity conditions. The annular flow in a microgravity environment is simpler than the one at normal gravity. A series of common models was presented: Homogenous model, Wheeler model, the Lockart-Marinelli-Chisholm model, and Annular Flow Model/ Chen Model.

CHAPTER IV

EXPERIMENTAL RESULTS AND PRESSURE DROP MODELING

4.1 INTRODUCTION

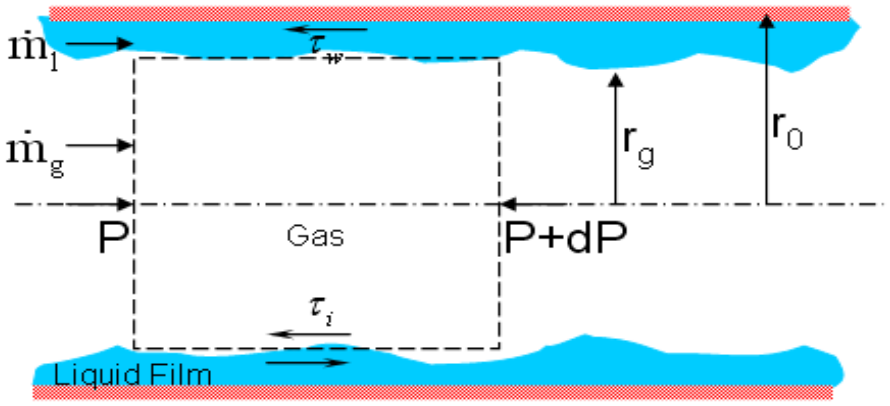

Figure 4.1: Control volume for analysis of two-phase annular flow

The mathematical model is developed based on the following assumptions (Figure 4.1)[23]:

- The flow is fully developed and steady.
- The liquid film is thin compared to the tube diameter.
- The shear stress in the liquid film is assumed constant and is equal to the interfacial shear stress.
- The effect of deposition and entrainment on liquid flow is neglected.
- Physical properties of the fluids are constant.

4.2 PRESSURE DROP MODEL

The interfacial shear stress on the surface between the liquid and vapor phase can be determined by using the momentum conservation equation

$$\tau_i = \frac{1}{2} f_i \rho_g \left(u_g - u_i\right)^2 \tag{4.1}$$

Near microgravity conditions, the interfacial velocity is much smaller than the vapor velocity and can be neglected, giving

$$\tau_i = f_i \frac{1}{2} \rho_g u_g^{\,2} = f_i \frac{1}{2} \frac{\rho_g j_g^{\,2}}{\alpha^2} \tag{4.2}$$

In two-phase flow, the void fraction is defined as the ratio of the vapor cross section area and the total cross section area:

$$\alpha = \frac{r_g^{\,2}}{r_0^{\,2}} \tag{4.3}$$

The vapor pressure gradient is determined by using the momentum equation neglecting acceleration and gravity terms at the interface

$$-\frac{dP}{dz} = f_i \frac{\rho_g}{r_g} \left(\frac{j_g}{\alpha} \right)^2 \tag{4.4}$$

The void fraction is substituted in Equation 4.4; the pressure gradient is given as

$$-\frac{dP}{dz} = f_i \frac{\rho_g j_g^{\,2}}{r_0} \frac{1}{\alpha^{2.5}} \tag{4.5}$$

The total pressure drop is determined by integrating Equation 4.5 over the length of the actual channel

$$\Delta P = \left(\frac{2 f_i L}{D} \right) \left(\frac{\rho_g j_g^{\ 2}}{\alpha^{2.5}} \right) \tag{4.6}$$

The interfacial friction factor and the void fraction are unknowns in Equation 4.6. Most researchers correlated either void fraction or film thickness through an iteration process. The unknown values were guessed at first, and then the iteration process was repeated until the calculated pressure drop and the measured pressure drop differed by a small tolerance. However, the iteration process was very computer intensive. With benefit of void fraction and film thickness measurements, the new empirical correlations of the interfacial friction factor and void fraction can be correlated more accurately.

4.2.1 Develop an Empirical Correlation for Void Fraction

The void fraction is one of the most important parameters used to characterize two phase flows and is the key physical value for predicting the two-phase pressure drop. In general, the void fraction may be a function of the fluid properties, channel geometry and two-phase flow rate. In fact, the void fraction is also presented as a function of the Martinelli parameter for two-phase adiabatic flows because the Martinelli parameter (X_{tt}) contains different physical parameters such as the liquid and vapor densities, the liquid and vapor viscosities and the mass quality.

$$\alpha = f\left(X_{tt}\right) \tag{4.7}$$

The void fraction correlation can also cast in the general form as given by (Van Carey, 2008)[24]:

$$\alpha = \left[1 + B\left(\frac{1-x}{x}\right)^{n_1}\left(\frac{\rho_g}{\rho_l}\right)^{n_2}\left(\frac{\mu_g}{\mu_l}\right)^{n_3}\right]^{-1} \tag{4.8}$$

The unknown values such as n_1, n_2, n_3, and B can be determined by fitting the experimental data to the correlation in the Equation 4.8.

Lockhart and Martinelli (1949) first attempted to predict the void fraction in a smooth tube.

$$\alpha = \left[1 + 0.18\left(\frac{1-x}{x}\right)^{0.6}\left(\frac{\rho_g}{\rho_l}\right)^{0.33}\left(\frac{\mu_l}{\mu_g}\right)^{0.07}\right]^{-1} \tag{4.9}$$

The homogeneous model is the simplest one for calculating void fraction in two-phase flow, in which the vapor and liquid phases are treated as a homogeneous mixture flowing with same velocity.

$$\alpha = \left[1 + \left(\frac{1-x}{x}\right)\left(\frac{\rho_g}{\rho_l}\right)\left(\frac{\mu_l}{\mu_g}\right)\right]^{-1} \tag{4.10}$$

Baroczy (1966) conducted experiments for isothermal, two-phase of liquid mercury-nitrogen and water-air and presented void fraction data as a function of the Lockhart and Martinelli parameter.

$$\alpha = \left[1 + \left(\frac{1-x}{x}\right)^{0.74}\left(\frac{\rho_g}{\rho_l}\right)^{0.65}\left(\frac{\mu_l}{\mu_g}\right)^{0.13}\right]^{-1} \tag{4.11}$$

Thom (1964) obtained an empirical relationship between quality and void fraction based on the assumption that the slip ratio is constant at a given pressure.

$$\alpha = \left[1 + \left(\frac{1-x}{x}\right)\left(\frac{\rho_g}{\rho_l}\right)^{0.89}\left(\frac{\mu_l}{\mu_g}\right)^{0.18}\right]^{-1} \tag{4.12}$$

Wallis (1969) obtained the correlation of void fraction at low pressure using the data of Lockhart and Martinelli.

$$\alpha = \left[1 + \left(\frac{1-x}{x}\right)^{0.72}\left(\frac{\rho_g}{\rho_l}\right)^{0.40}\left(\frac{\mu_l}{\mu_g}\right)^{0.08}\right]^{-1} \tag{4.13}$$

For engineering designs, selection of a two-phase flow model should be done carefully. The homogeneous model yields reasonably accurate results only for limited circumstances where the slip velocity between phases is small. The Lockhart-Martinelli model yields reasonably accurate results for a wide variety of two-phase flow circumstances in round tubes and simple channel geometries. The Baroczy model is correlated from a very large database and is more complex than the others, but it provides the best accuracy for a wide variety of circumstances (Van P. Carey, 2008). Wheeler (1992) and Tandon (1985) predicted that the void fraction for the annular flow is a function of both the liquid Reynolds number and the Martinelli parameter. Their models had improvements over models above because they included the effect of the mass flux and the wall friction.

New void fraction correlation

Assume the void fraction can be written in the general form as given by:

$$\alpha_{model} = \left[1 + p_1\left(\frac{1-x}{x}\right)^{p_2}\left(\frac{\rho_g}{\rho_l}\right)^{p_3}\left(\frac{\mu_g}{\mu_l}\right)^{p_4}\right]^{-1} \tag{4.14}$$

The unknowns $\vec{p}(p_1, p_2, p_3, p_4)$ in Equation 4.14 can be determined by linear least squares regression. The idea behind the least squares method is to sum the distance between points and the line and minimize the total error. The total least squares error which will be required for minimization is given by:

$$E(\alpha_{measured}, \alpha_{model}) = \sum_{i=1}^{n} (\alpha_{measured}(i) - \alpha_{model}(i))^2 \tag{4.15}$$

A Matlab code was developed such that one can provide an initial guess for $\vec{p}(p_1, p_2, p_3, p_4)$ to calculate the total least squares error. The iteration process updates values of $\vec{p}(p_1, p_2, p_3, p_4)$ continuously until the total least squares error is minimized. Then, the code is terminated and returns the final values of $\vec{p}(p_1, p_2, p_3, p_4) = (1.1809, 0.646, 1.2135, 0.7989)$ and $E(\alpha_{measured}, \alpha_{model}) = 0.0087$.

The new empirical correlation for void fraction has the same form used by Lockhart and Martinelli (1949), Thom (1964), Baroczy (1966) and Wallis (1996), but with different coefficients and power dependence.

$$\alpha = \left[1 + 1.1809 \left(\frac{1-x}{x} \right)^{0.646} \left(\frac{\rho_g}{\rho_l} \right)^{1.2135} \left(\frac{\mu_l}{\mu_g} \right)^{0.7989} \right]^{-1} \tag{4.16}$$

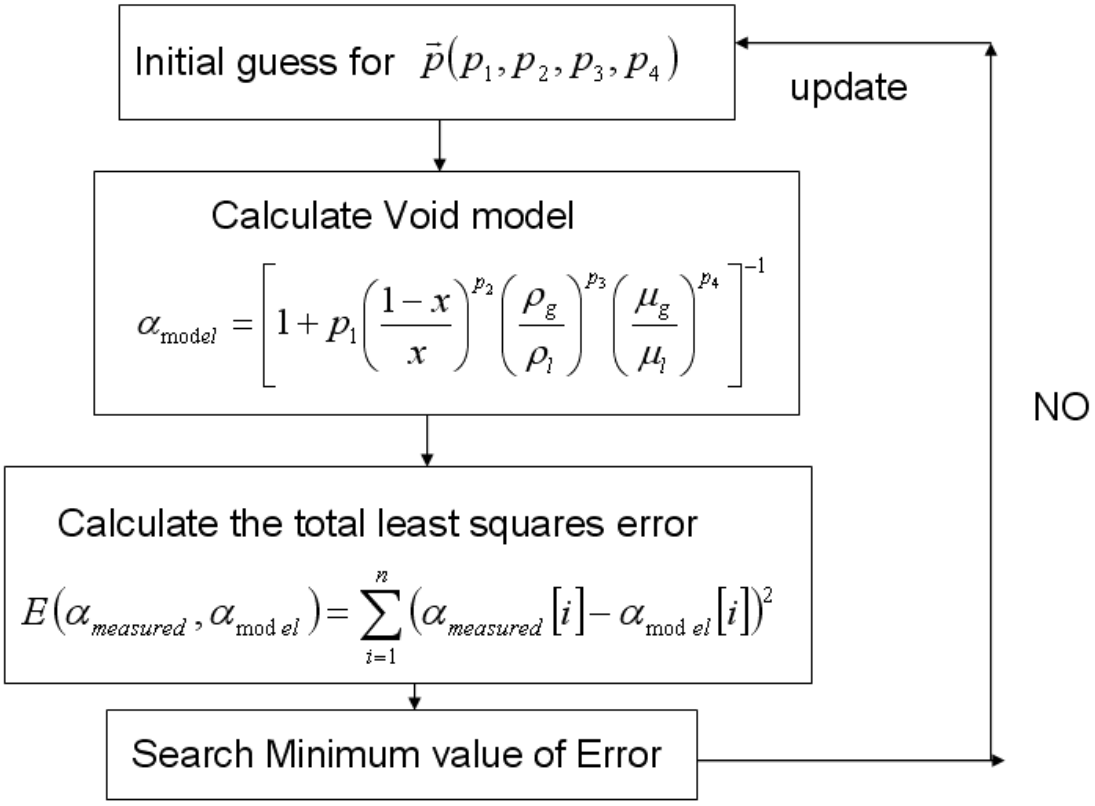

Figure 4.2: Linear least squares regression for the void fraction

A series of void fraction models was evaluated and plotted in Figure 4.2. The measured void fraction varied from 0.52 to 0.92 for annular flow under microgravity conditions.

Table 4.1: Void average error (Creare, 2001)

Model	Void Average Error (%)
New void (2009)	**-0.02**
Wheeler (1992)	1.29
Wallis (1969)	-20.03
Lockhart and Martinelli (1949)	9.55
Baroczy (1966)	-1.18
Thom (1964)	5.75
Zivi (1964)	0.42
Homogeneous	19.23

The results of the void average error from different models were shown in Table 4.1. The void fraction predicted by Wheeler (1992) was in a good agreement with the measured void fraction. This is expected because the two-phase flow test bed in the present study is a new version of that used by Wheeler (1992) with major modifications including void fraction and film thickness measurements. The homogeneous model overpredicts the data because there is slip velocity between phases under microgravity. Zivi (1964) and Baroczy (1949) which are correlated from a very large database accurately provided average errors to be 0.42 % and 1.18 %.

Figures 4.3 shows all of measured void fraction data obtained in the current program compared with the prediction of the new empirical void fraction correlation, and correlations from Wheeler (1992), Wallis (1969), Lockhart and Martinelli (1949),

Baroczy (1966), Thom (1964), Zivi (1964) and the homogeneous correlation. Many of these correlations accurately predict the measured void fraction data. However, most of void fraction data are not predicted well using Wallis correlation and homogeneous correlation.

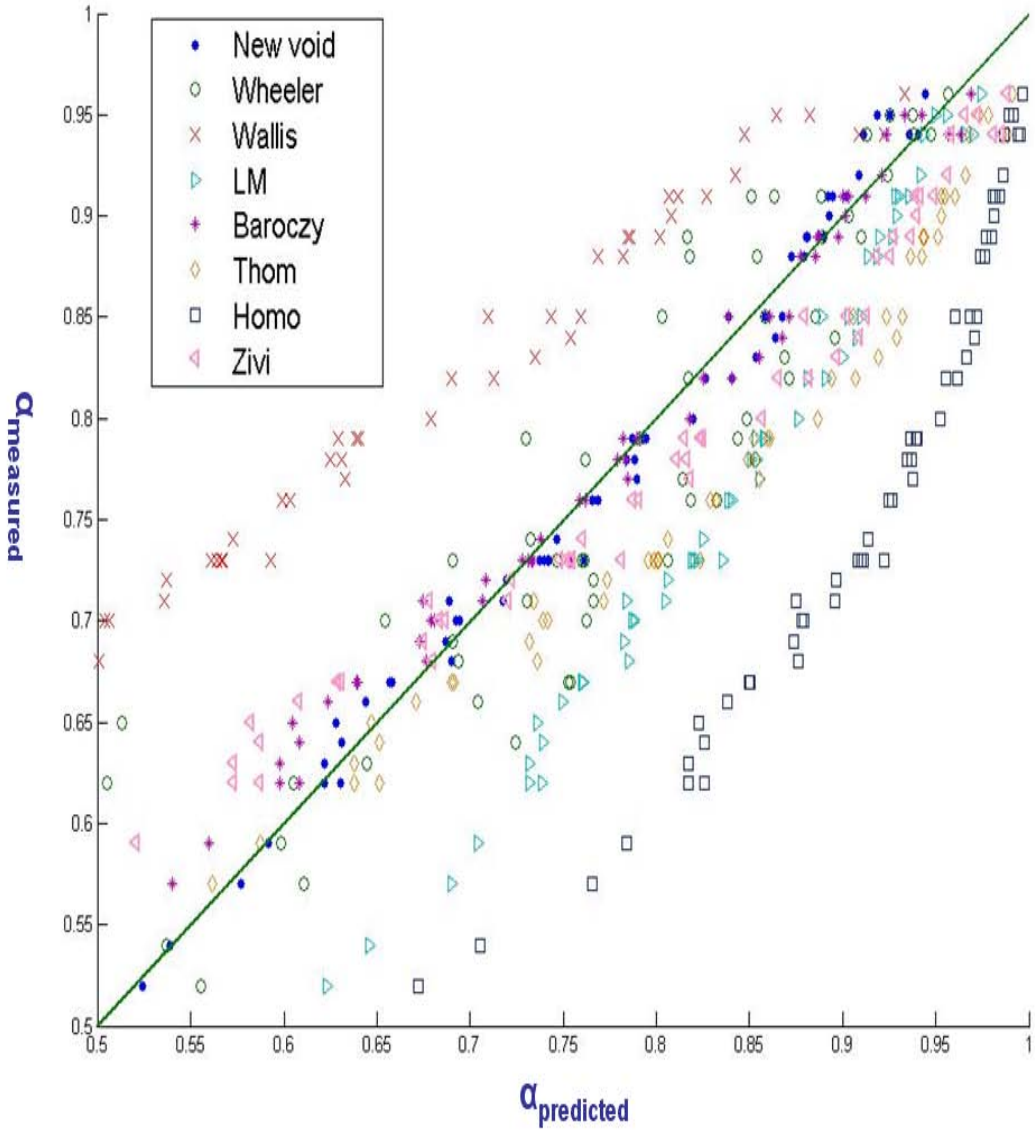

Figure 4.3: Comparison of void fraction under microgravity

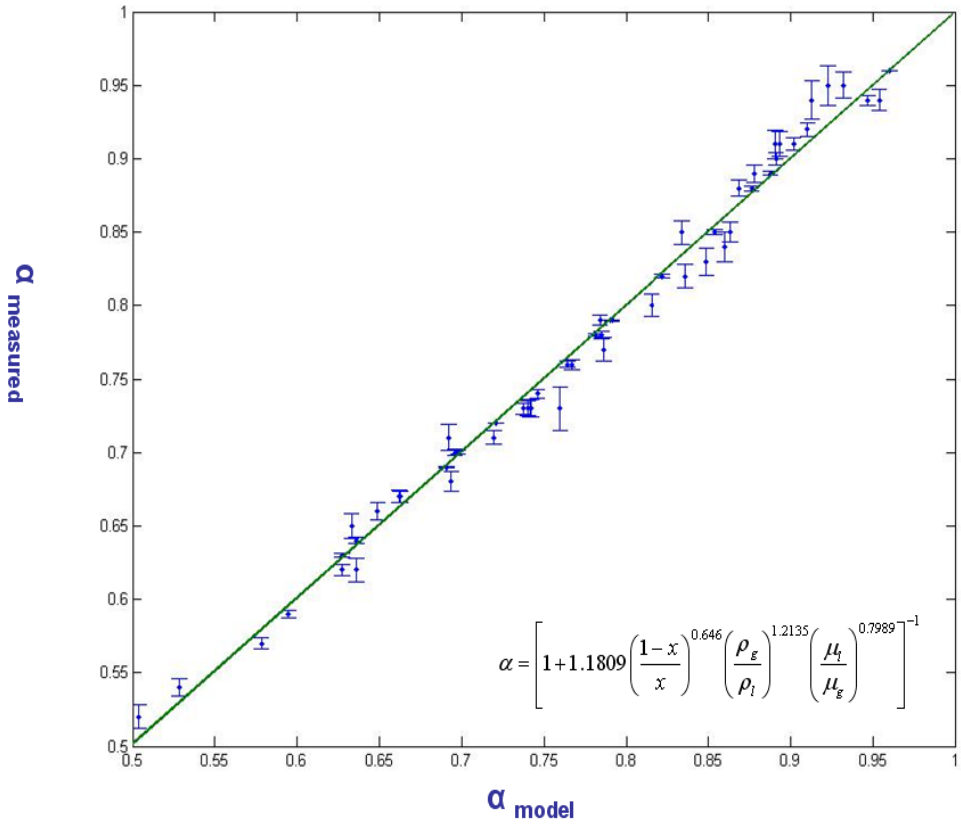

Figure 4.4: Comparison of measured void fraction and predicted void fraction

It can be seen from Figure 4.4 that small error bars supports the validity of the experimental void fraction results. Furthermore, the new model accurately predicts measured void fractions of 0.02 % average error.

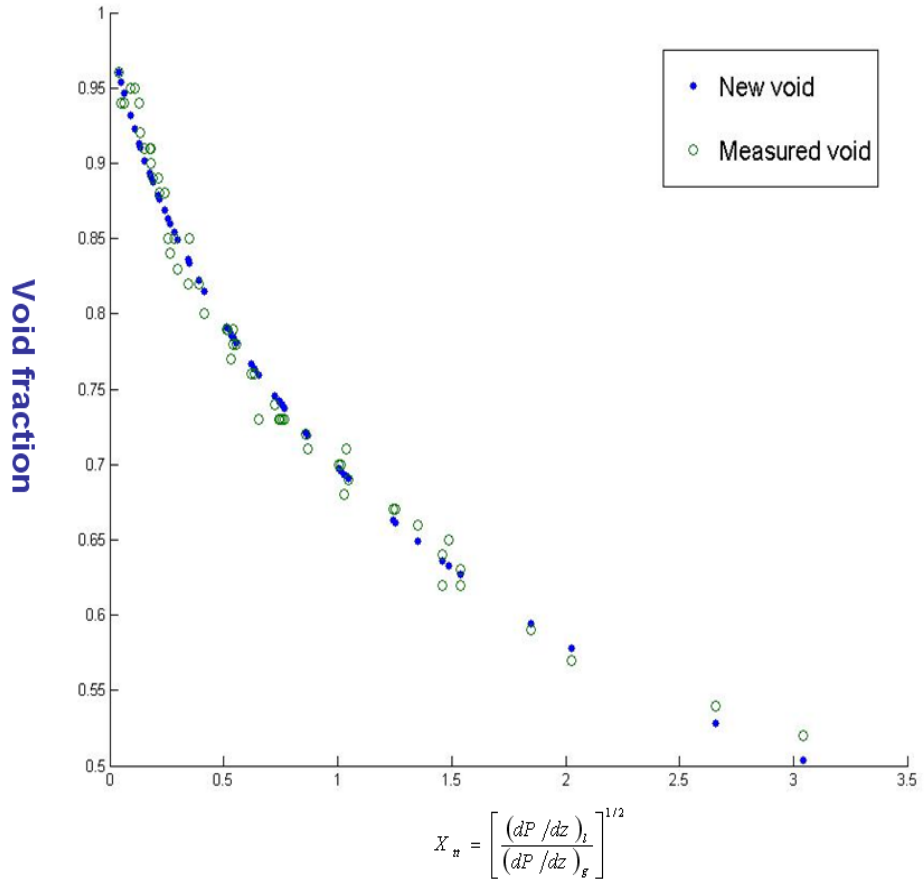

Figure 4.5: Void fraction as a function of Martinelli parameter

Figure 4.5 shows the void fraction as a function of Martinelli parameter. The void fraction decrease with increasing the Martinelli parameter. Most correlations can not predict the void fraction accurately at a high Martinelli parameter except correlations from Nguyen (2009), Wheeler (1992) and Baroczy (1966).

4.2.2 Develop an Empirical Correlation for Interfacial Friction Factor

In general, the interfacial friction factor may be a function of the film thickness, quality, mass flux and the tube diameter, $f_i = f_i(\delta, x, G, D)$.However, many studies including those of Wallis (1969), Calvert and Williams (1958), Mantzouranis (1959), Hewitt and Hall-Taylor (1970), Asali (1985), and Lopes and Duckler (1986) concluded that the interfacial friction factor is a direct function of the liquid film thickness (Collier, 1994)[25].

$$f_i = f(\delta/D) = f_g\left\{1 + B(\delta/D)^n\right\} \tag{4.17}$$

where f_g is the single phase friction factor in absence of the liquid film and is assumed to have the constant value of f_g = 0.005, and unknown values B and n.

The simplest correlation is proposed by Wallis (1969)[26] for the case of no entrainment and ignoring the interface velocity for air/water at 1-g:

$$f_i = f_g\{1 + 300(\delta/D)\} \tag{4.18}$$

Moeck (1970) also developed a similar form of interfacial factor correlation for the flow in the disturbance wave region for air/water:

$$f_i = f_g\left\{1 + 1458(\delta/D)^{1.42}\right\} \tag{4.19}$$

Chen (1989) developed his interfacial friction factor correlations in the annular flow regime from R-114 data at low gravity:

$$f_i = f_g\left\{1 + 11.7(\delta/D)^{0.39}\right\} \tag{4.20}$$

Later, the correlation of Wallis was modified by Fore (2000) for a better fit to very small film thickness data obtained from several past studies[27,28,29]

$$f_i = f_g\{1+300(\delta/D-0.0015)\} \tag{4.21}$$

All of the interfacial friction factor correlations shown above were developed through an iteration process which is very computer intensive. With the benefit of film thickness measurements, one can develop a more accurate empirical correlation for the interfacial friction factor as a function of liquid film thickness δ/D that could acceptably predict most of the experimental data collected for two-phase flow under microgravity conditions.

New interfacial friction factor correlation

The linear least squares regression flow chart is shown in Figure 4.6

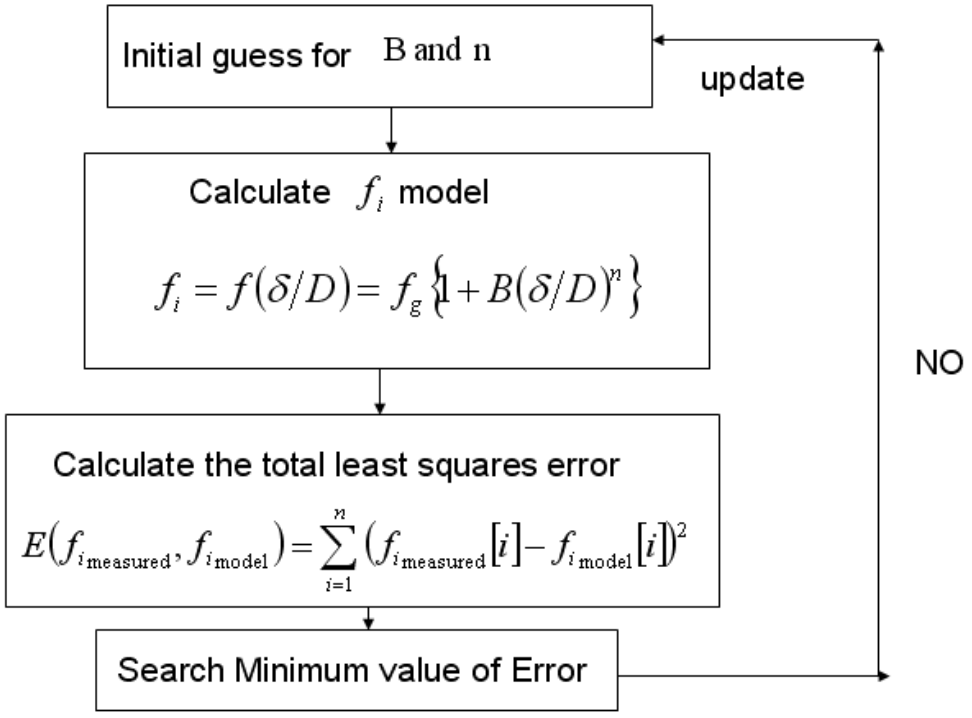

Figure 4.6: Linear least squares regression for the interfacial friction factor

Using the linear least squares regression on the reduced gravity data, the empirical correlation for the interfacial friction factor is

$$f_i = 0.005\left\{1 + 50.68\left(\delta/D\right)^{0.88}\right\} \tag{4.22}$$

The new interfacial friction factor has a simple expression that relates the interfacial friction factor with the film thickness and the tube diameter.

The results of the interfacial friction factor average error from different models were shown in Table 4.2. Interfacial friction factors predicted by Nguyen (2009), Wheeler (1992) and Chen (1989) were in a good agreement with interfacial friction factors which are calculated by the measured void fraction and measured pressure drop.

Table 4.2: fi average error (Creare, 2001)

Model	f_i Average Error (%)
New model (2009)	**11.01**
Wallis (1996)	258.78
Homogeneous	258.78
Lockhart and Martinelli (1949)	258.78
Chen (1989)	20.74
Moeck (1970)	379.47
Wheeler (1992)	21.02

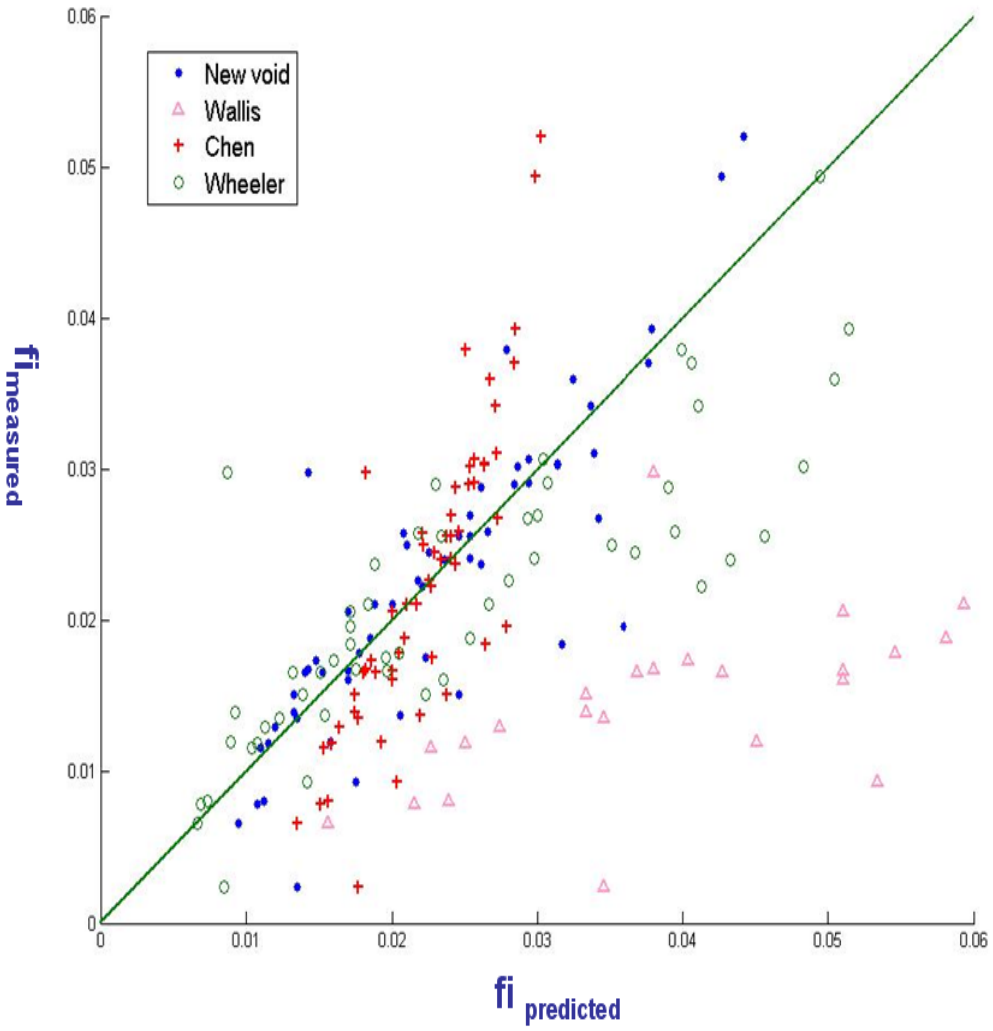

Figure 4.7: Comparison of interfacial friction factor under microgravity

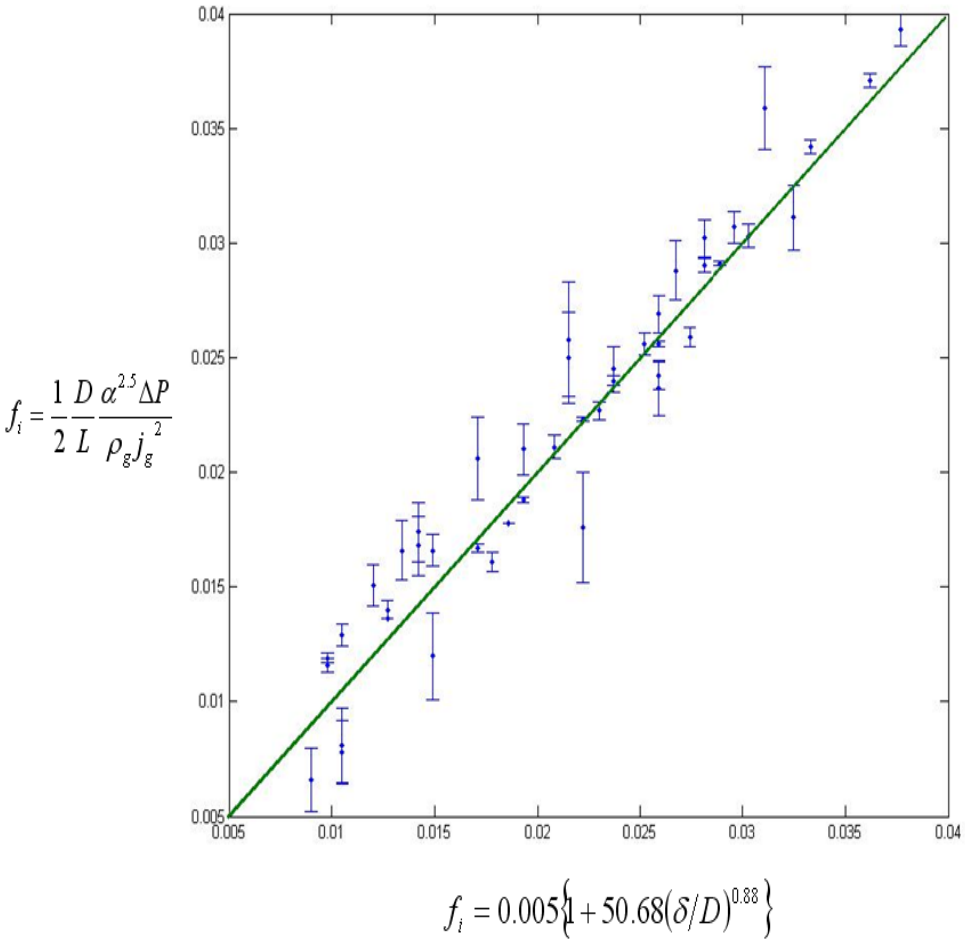

Figure 4.8: Comparison of measured void fraction and predicted void fraction

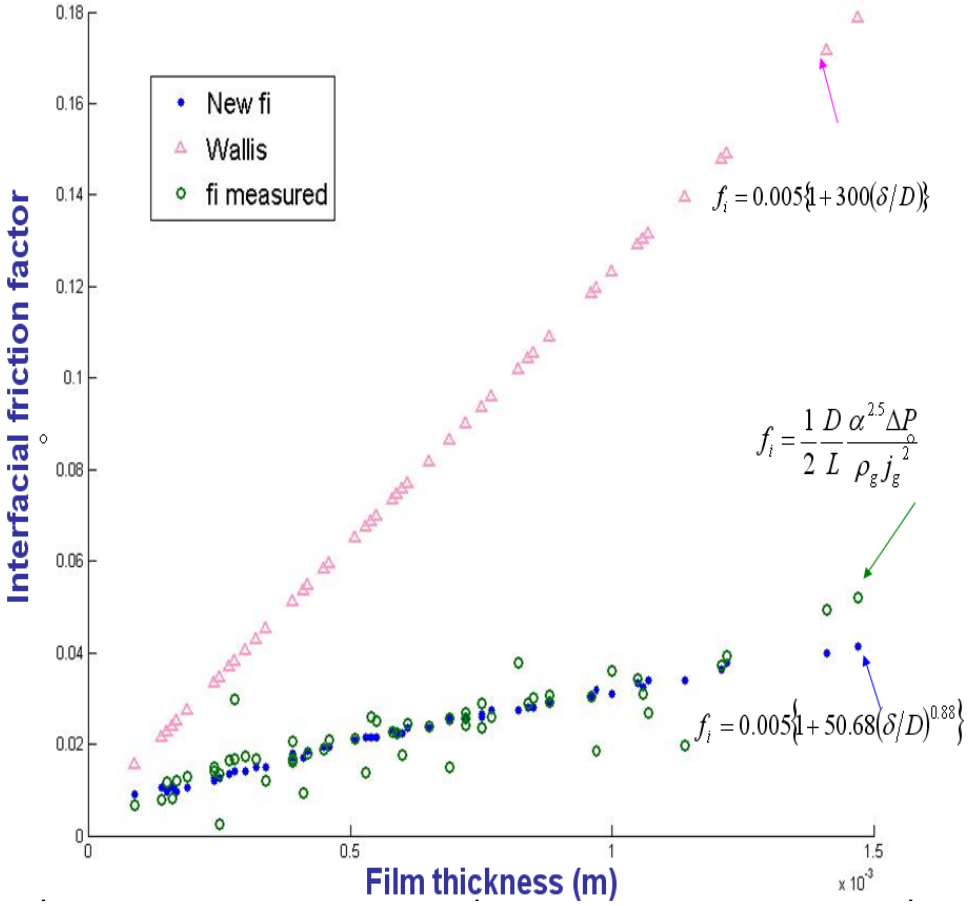

Figure 4.9: Interfacial friction factor as a function of film thickness

Figures 4.7, 4.8 and 4.9 show that the Wallis correlation overpredicts the reduced acceleration experimental interfacial friction factor by as much as 258 %. This result is expected because, in vertical upflow, a greater interfacial shear must exist to counter the body force on the liquid film due to gravity. This increased shear contributes to a rougher vapor-liquid interface which means a larger interfacial friction factor. In zero gravity, the only opposing force is the tube shear on the liquid, thus the vapor shear required to drive the liquid is less, leading to a smoother interfaces which means a

smaller interfacial friction factors (Wheeler, 1990). As the results of that, Chen (1989) and Wheeler (1992) predicted the reduced acceleration experimental interfacial friction factor accurately with the average error to be 20%. Furthermore, as the film thickness is increased, the interfacial friction factor is increased with a linear dependence.

4.3 PREDICTING THE PRESSURE DROP

Once again, the friction pressure drop can be expressed as:

$$\Delta P = 2 f_i \left(\frac{L}{D} \right) \frac{G^2 x^2}{\rho_g \alpha^{2.5}} \tag{4.23}$$

The interfacial friction factor was chosen from Nguyen (2009), Wallis (1996), Wheeler (1990), and Chen (1989) correlations to predict the pressure drop. Since most two-phase flow pressure drop experiments do not measure the void fraction or the film thickness, it is necessary to use a void fraction correlation that can cover a wide range of data to predict the pressure drop.

Table 4.3: ΔP average error from Creare

Model	DP average error (%)
New model (2009)	**11.2002**
LM (1949)	134.232
Wheeler (1992)	15.9315
Chen (1989)	20.7418
Homogeneous	-3.6937

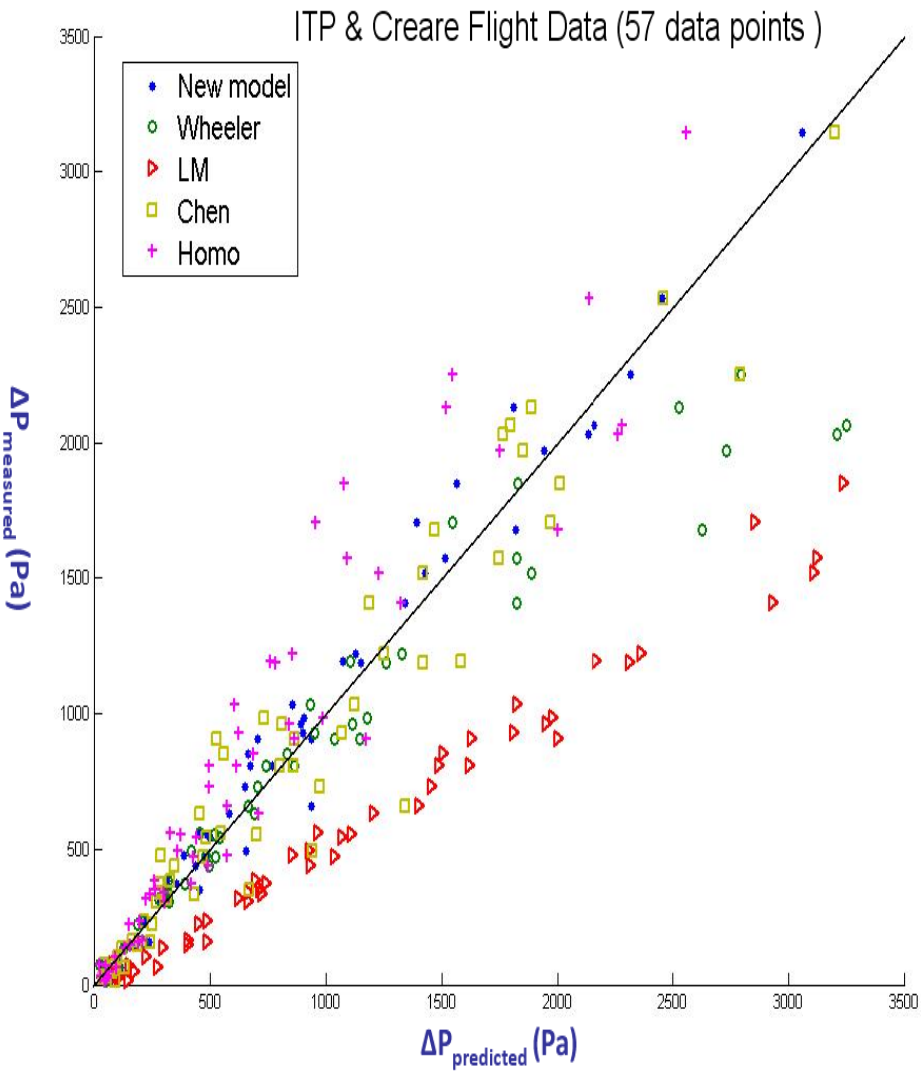

Figure 4.10: Comparison of two-phase pressure drop under 0-g (Creare, 2001)

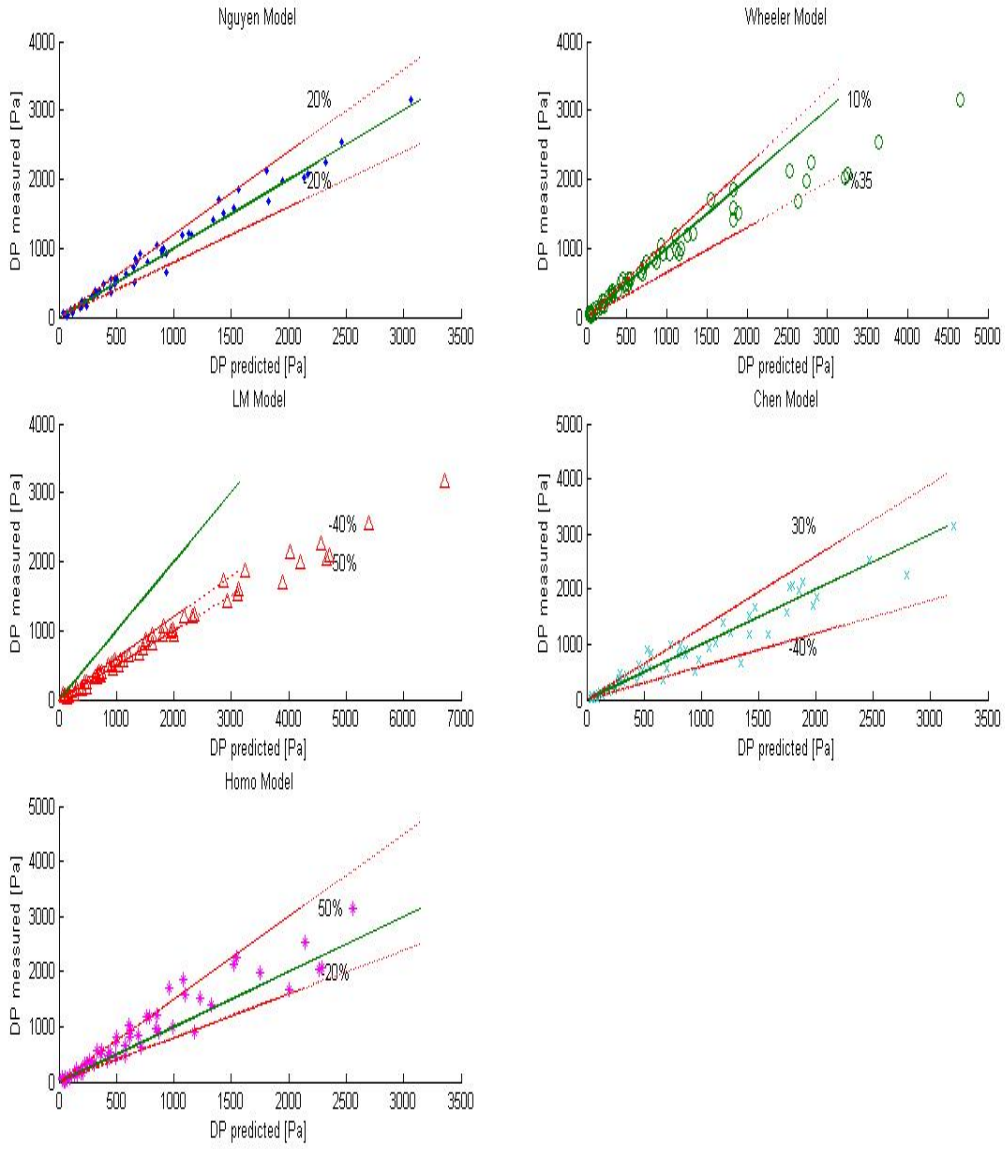

Figure 4.11: Two-phase pressure drop models under 0-g (Creare, 2001)

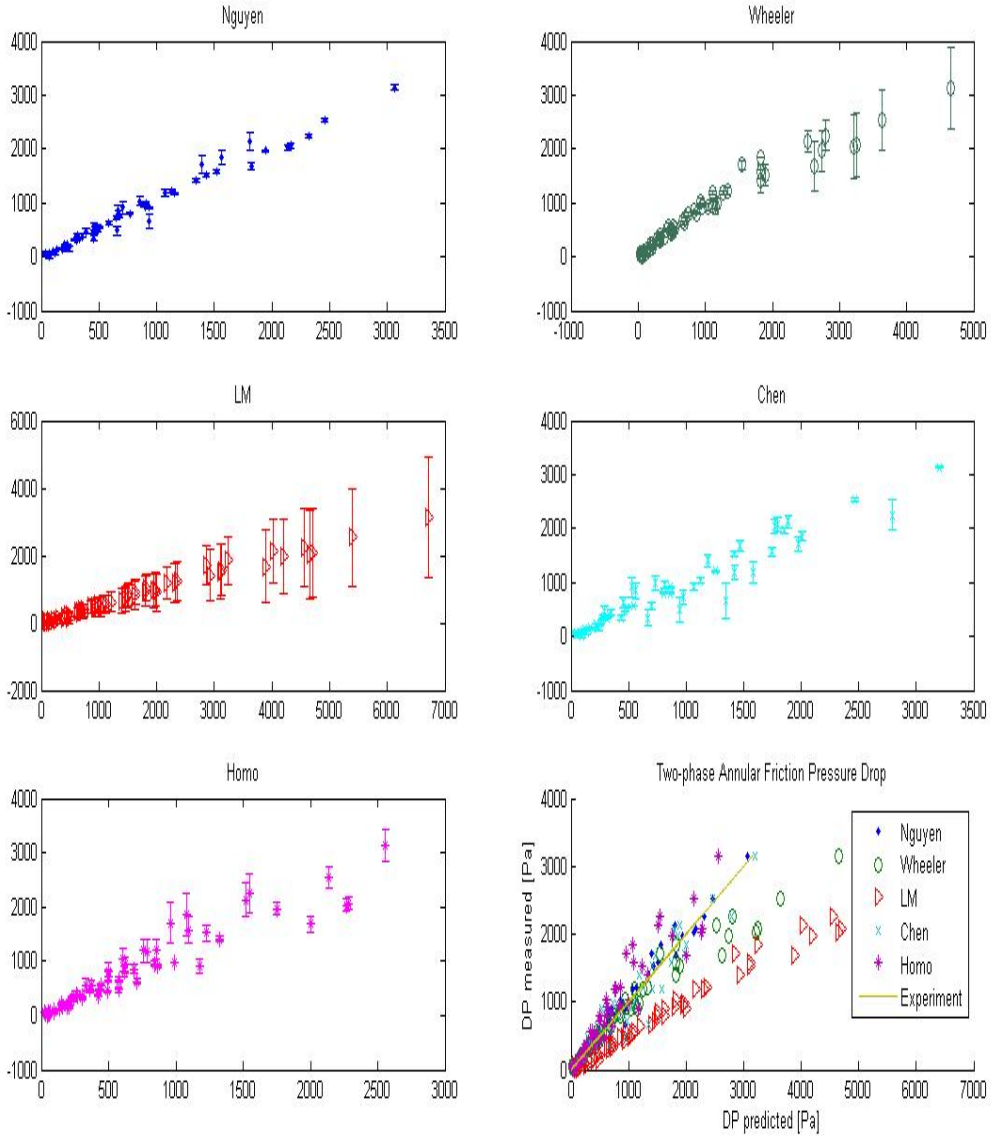

Figure 4.12: Two-phase pressure drop models with error bars (Creare, 2001)

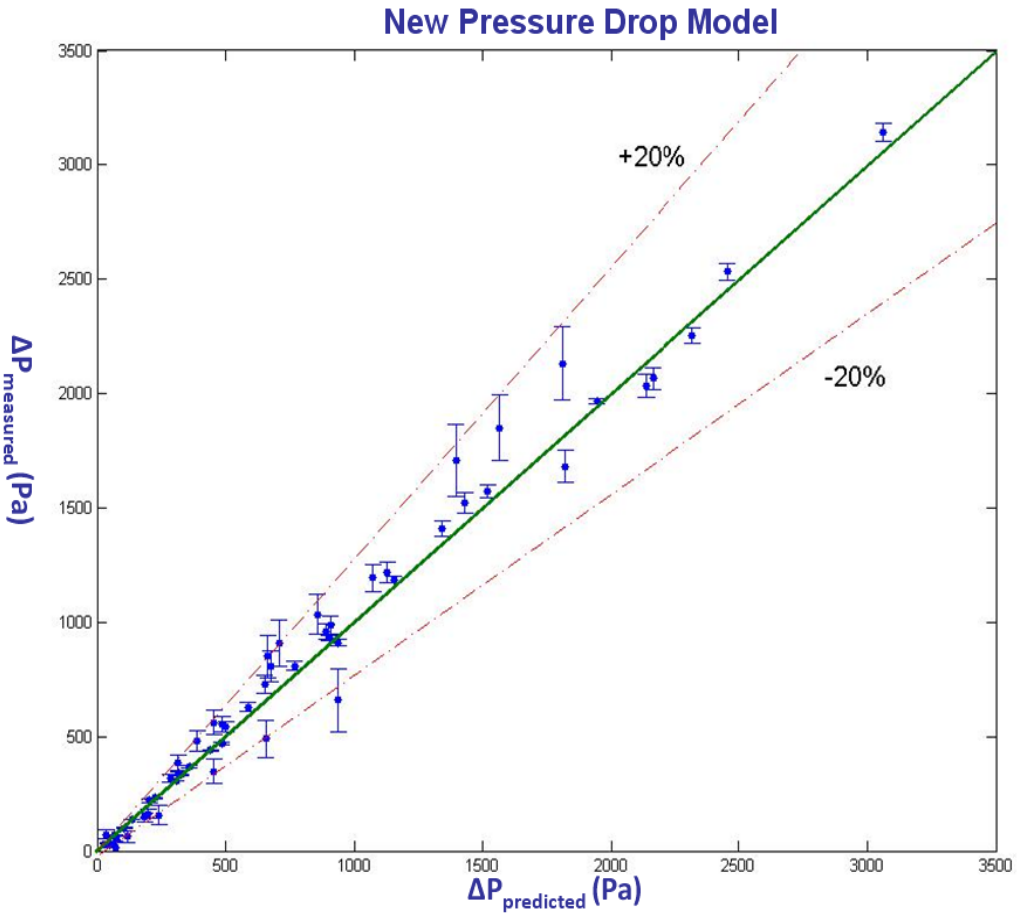

Figure 4.13: New two-phase pressure drop model (Creare, 2001)

Figures 4.10 and 4.11 and Table 4.3 show that the Lockhart-Martinelli model overpredicts all values of measured pressure drop while the homogeneous model and the Chen model lightly underpredicts some data. The Wheeler model is the second most accurate model to predict the measured data of the average error of 16 % (Figure 4.12). The new model is the optimal model for predicting the two-phase friction pressure drop in annular regimes. Figure 4.13 shows that the majority of the data fall within +-20% of

the proposed correlation and the average error is 12 %. The small error bar in Figure 4.13 indicates that the new model accurately predicts the pressure drop with a low standard deviation.

4.4 PRESSURE DROP MODEL APPLICATION

The annular two-phase friction pressure drop can be predicted by the new model requiring only knowledge of the length and diameter of the tube, liquid and vapor mass flow rates and properties of the working fluid.

The model is valid under these assumptions:

- The liquid is thin compared with the tube diameter.
- The interface between vapor and liquid is smooth.
- Constant shear stress in liquid film, and no deposition or entrainment on the liquid flow.
- Void fraction is from 0.5 to 0.9 for the annular flow regime

The pressure drop can be predicted with following steps:

1. Calculate the mass flux $G = \frac{\dot{m}_g + \dot{m}_l}{A}$

2. Calculate the mass quality $x = \frac{\dot{m}_g}{\dot{m}_g + \dot{m}_l}$

3. Calculate the superficial vapor and liquid velocities

$$j_g = \frac{Gx}{\rho_g} \ , \ j_l = \frac{G(1-x)}{\rho_l}$$

4. Identify whether the superficial vapor and liquid velocities fall into the annular flow regime using flow regime maps shown in Figure 14.

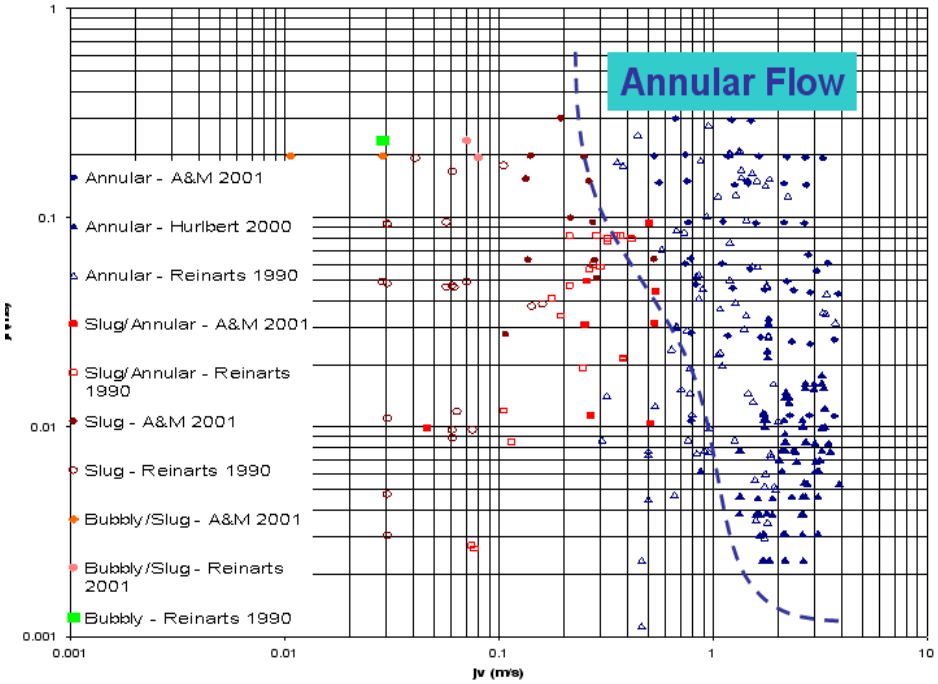

Figure 4.14: Flow regimes map

5. Calculate the void fraction using new correlation

$$\alpha = \left[1+1.1809\left(\frac{1-x}{x}\right)^{0.646}\left(\frac{\rho_g}{\rho_l}\right)^{1.2135}\left(\frac{\mu_l}{\mu_g}\right)^{0.7989}\right]^{-1}$$

6. Calculate the interfacial friction factor using new correlation

$$f_i = 0.005\left\{1+50.68\left(\delta/D\right)^{0.88}\right\} \qquad \text{where} \qquad \frac{\delta}{\mathrm{D}} = 0.23\left(1-\alpha\right)-0.0035$$

7. Calculate annular two-phase pressure drop

$$\Delta P = \left(\frac{2 f_i L}{D}\right)\left(\frac{\rho_g j_g^{\ 2}}{\alpha^{2.5}}\right)$$

4.5 PRESSURE DROP MODEL VALIDATION

The new pressure drop model was validated using Foster-Miller & ITP data collected over twelve flights aboard the KC-135 with working fluid R-12 (77 data points), Sundstrand data collected aboard the KC-135 with working fluid R-114 (43 data points) and Zhao and Rezkallah data aboard KC-135 with working fluid water and air (43 data points).The annular flow regime observations are plotted in Figure 4.15 as a function of vapor and liquid superficial velocities to compare the testing conditions among flight data sets. The summary of previous 0-g experiment is shown in Table 4.4.

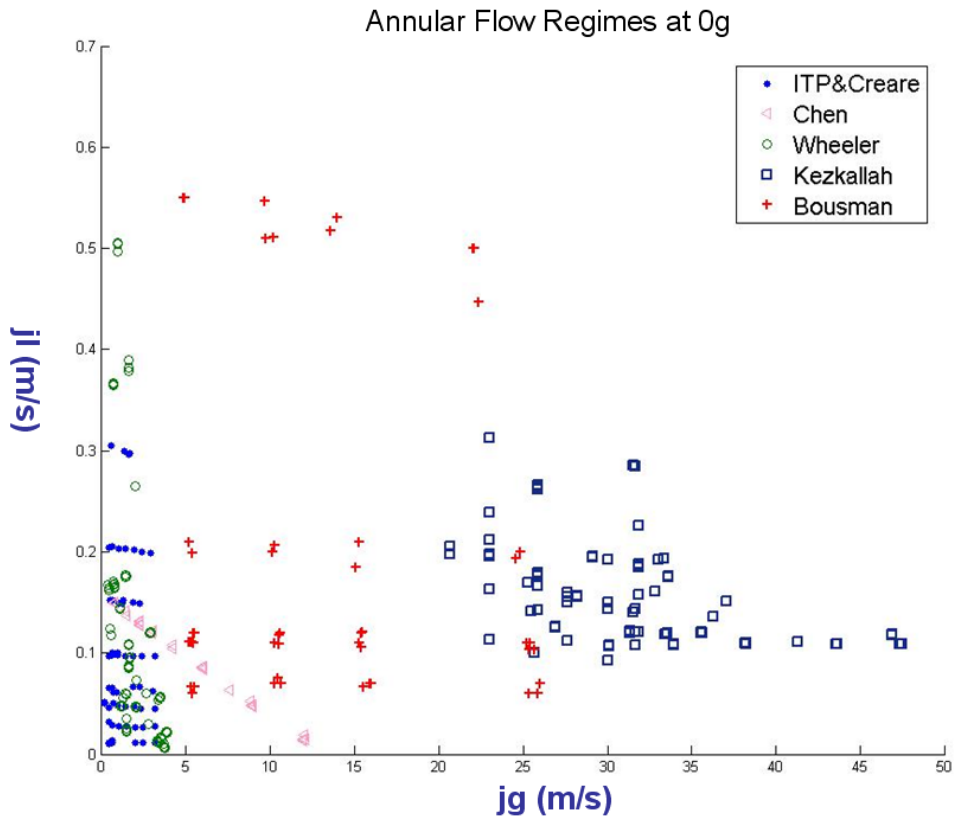

Figure 4.15: Annular flow regimes under microgravity

Table 4.4: Previous 0-g experiments

Authors	Date	Diameter mm	Length m	Vapor	Liquid	Regime	Pressure Drop ΔP	Void Fraction <α>	Film thickness δ
Chen&Downing	1988	15.8	1.83	R-114	R-114	S,A	Y		
Chen,Downing,Keshock & Al-Sharif	1989								
Wheeler	1992	10.5	1.22	R-12	R-12	A	Y		
Wheeler, Best, & Reinarts	1993								
Cherry & Rezkallah	1993	9.52	1.09	Air	Water	B,S,A	Y		
Zhao & Rezkallah	1994	9.52	1.09	Air	Water	B,S,A	Y		
Bousman	1995	12.7	0.64	Air	Water	B,S,A	Y	Y	
Bousman, McQuillen & Witte	1996	25.4	2.44		w/Glycerine	B,S,A	Y	Y	Y
Best & Creare	2000	12.7	1.63	R-12	R-12	S,A	Y	Y	Y

According to the Zhao and Rezkallah (1994) flight data, the annular flow regime presented at very high vapor superficial velocities compared with other researchers. Since the two-phase pressure drop is proportional to the square of vapor superficial velocity, the measured pressure drop is expected to be larger than the predicted pressure drops from different models.

4.5.1 Foster-Miller & ITP flight data (1900 – 1992) / Wheeler data (77 points)

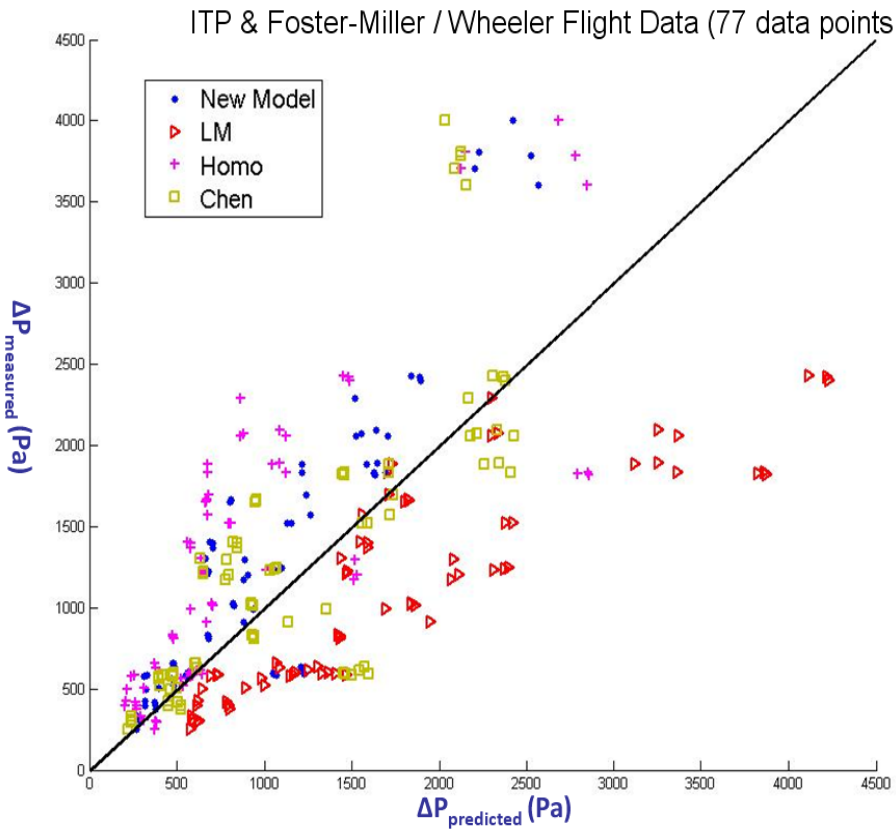

Figure 4.16: Two-phase pressure drop models under 0-g (Wheeler, 1992)

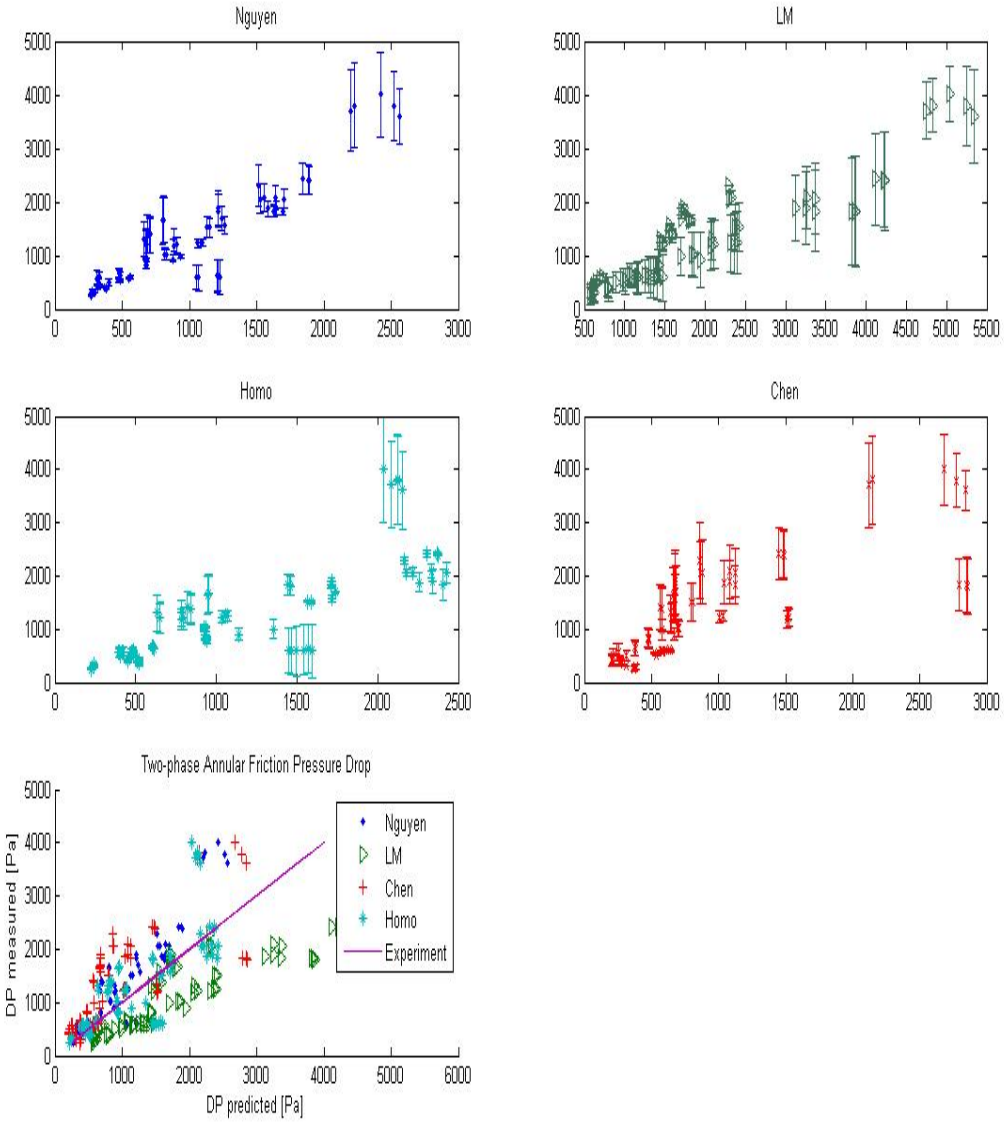

Figure 4.17: Two-phase pressure drop models with error bars (Wheeler, 1992)

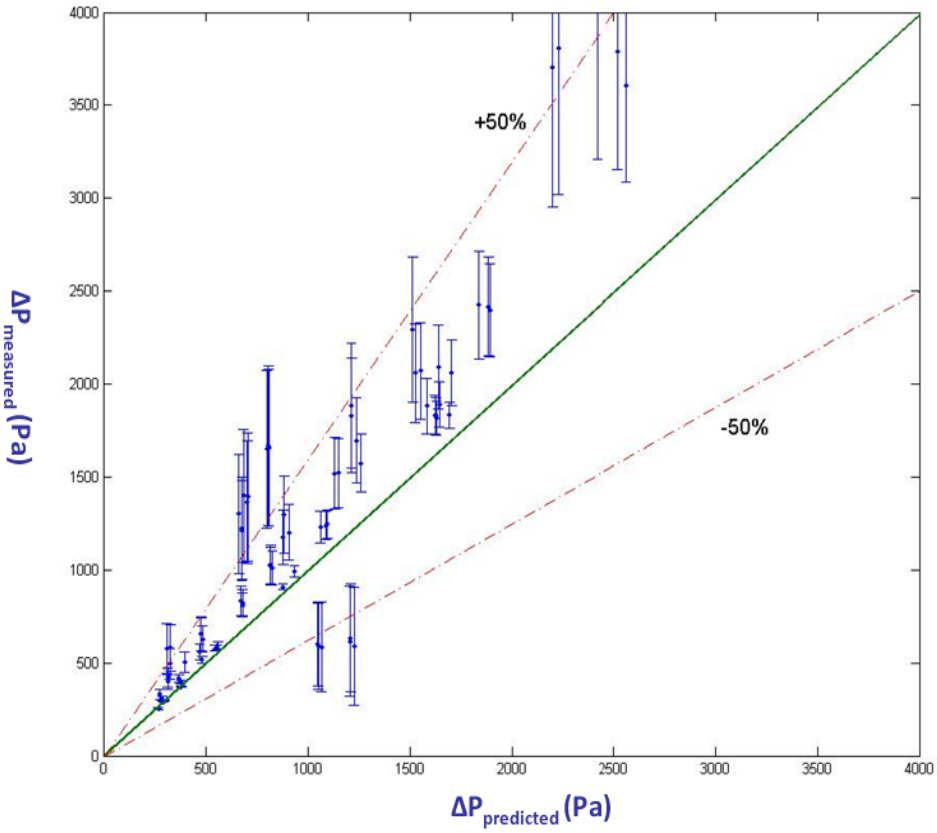

Figure 4.18: Prediction of two-phase pressure drop model on Wheeler data

The results shown in Figures 4.16, 4.17 and 4.18 indicate that the new model and Chen pressure drop model are only moderately successful. Most of data collected in Wheeler thesis lie within +- 50 % of the predicted pressure drop values. Again, the Lockhart-Martinelli model overpredicts all values of measured pressure drop. The results of predicted pressure drops from these models are very close to results from previous data of ITP & Creare (2001). It is expected because both experiments were conducted at a very close flow conditions and environments.

4.5.2 Sundstrand flight data (1987) / Chen and Downing data (43 points)

The pressure drop average errors are shown in Table 4.5. The comparison between measurement and prediction is shown in Figure 4.19.

Table 4.5: ΔP average error from Chen

Model	DP average error (%)
Nguyen (2009)	**18.4981**
LM (1949)	426.9582
Wheeler (1992)	197.9479
Homogeneous	53.4194

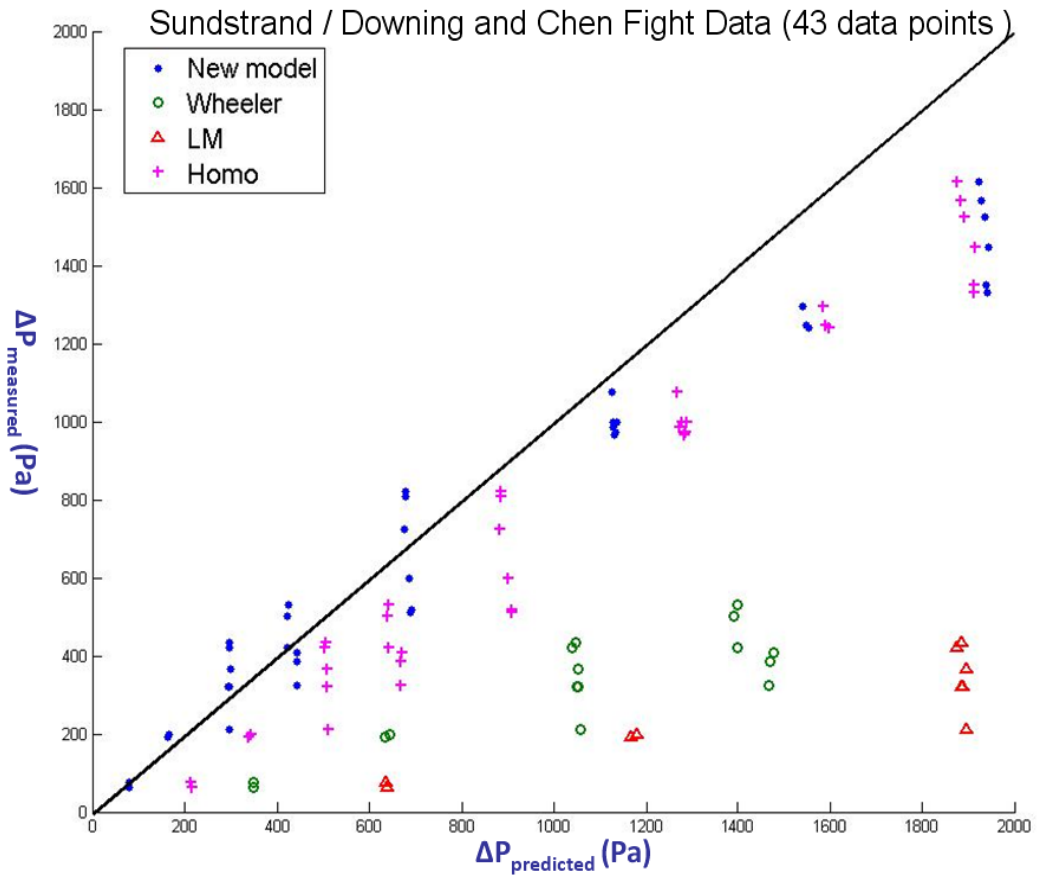

Figure 4.19: Two-phase pressure drop models under 0-g (Chen, 1989)

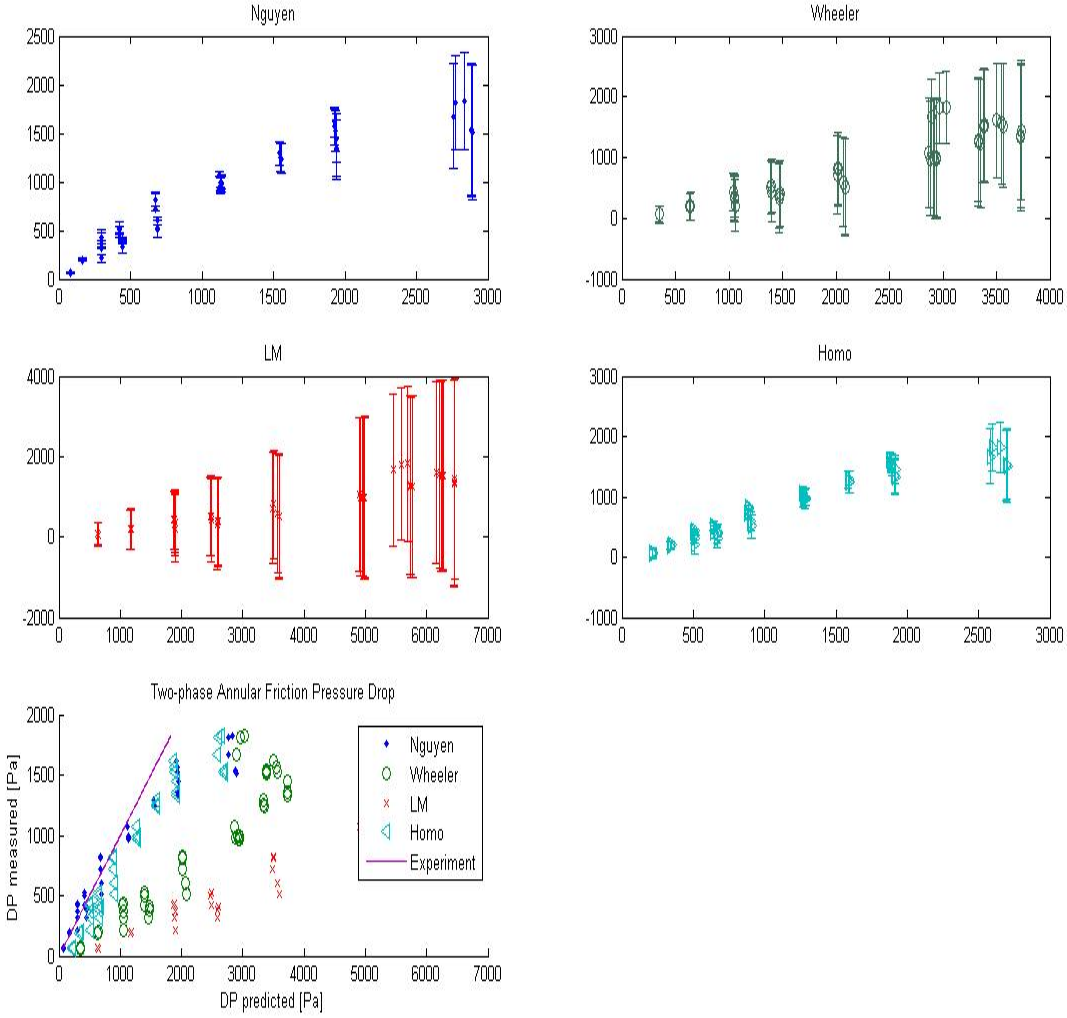

Figure 4.20: Two-phase pressure drop models with error bars (Chen, 1989)

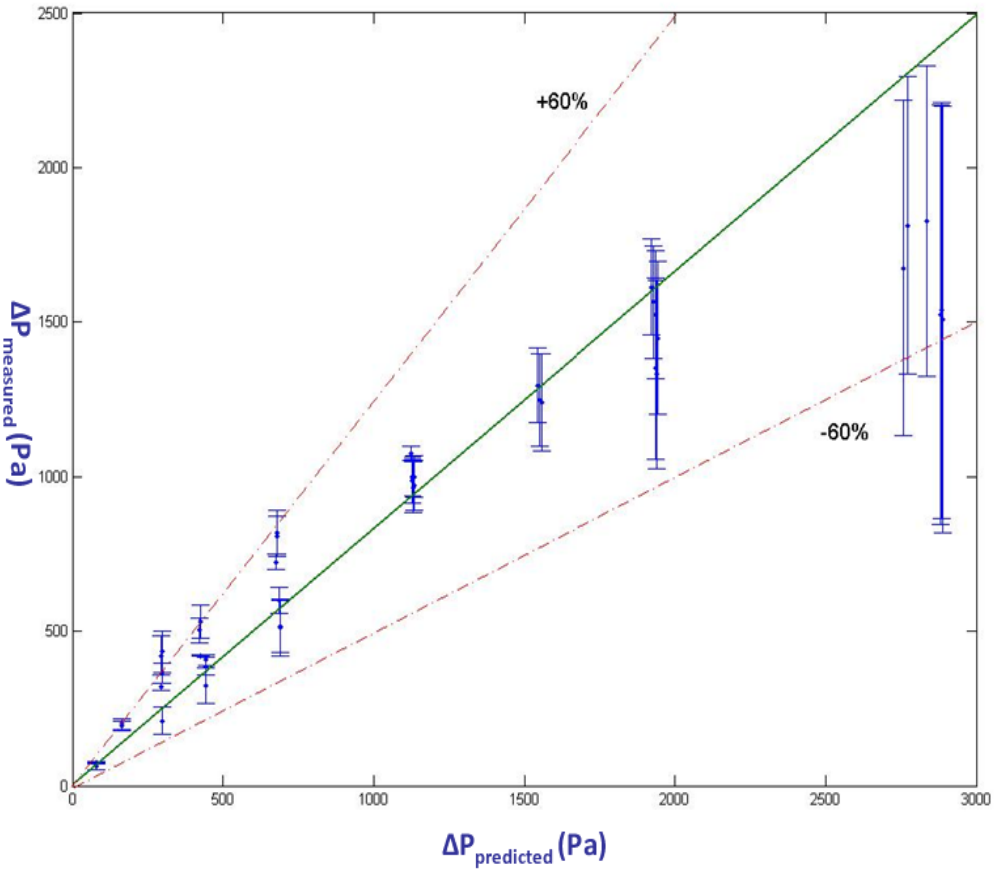

Figure 4.21: Prediction of two-phase pressure drop model on Chen data

The results shown in Figures 4.19, 4.20 and 4.21 indicate that the new model predicts the measured pressure drops more accurately compared with other models which overpredict the data.

4.5.3 Bousman flight data, 1994 (47 points)

The pressure drop average errors are shown in Table 4.6. The comparison between measurement and prediction is shown in Figure 4.22.

Table 4.6: ΔP average error from Bousman

Model	DP average error (%)
New model (2009)	**-24.8689**
LM (1949)	-66.8027
Wheeler (1992)	-52.1157
Chen (1989)	-94.8175
Homogeneous	-93.6551

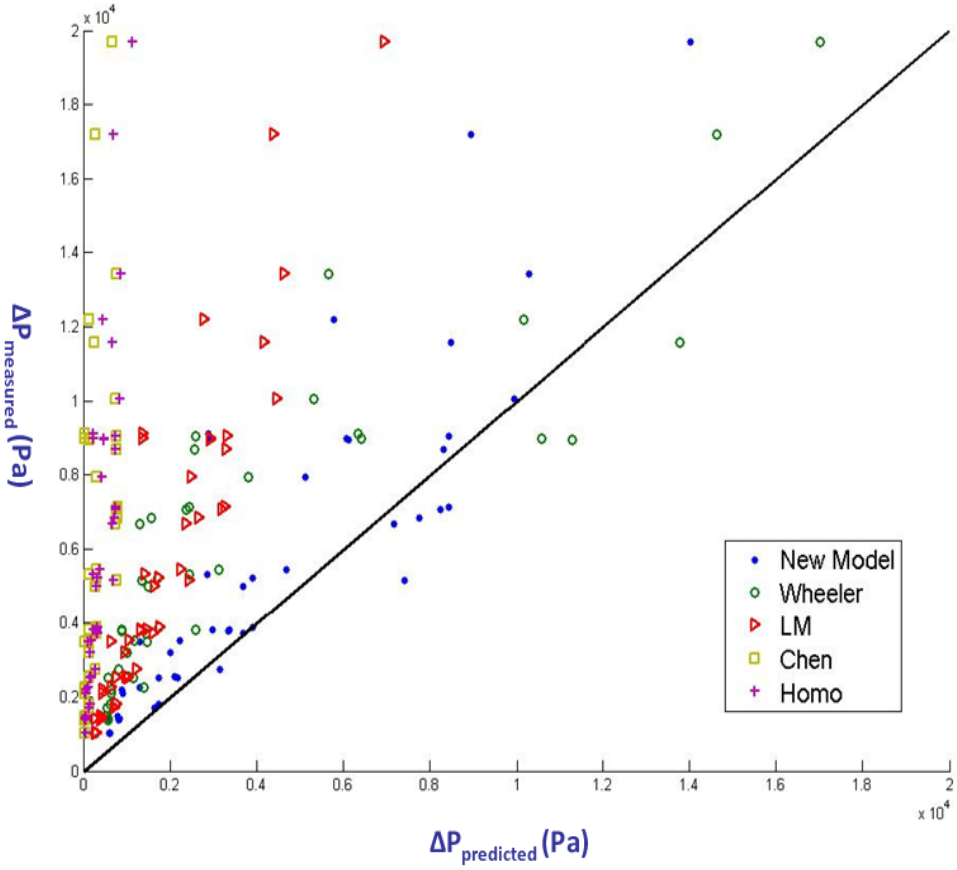

Figure 4.22: Two-phase pressure drop models under 0-g (Bousman, 1994)

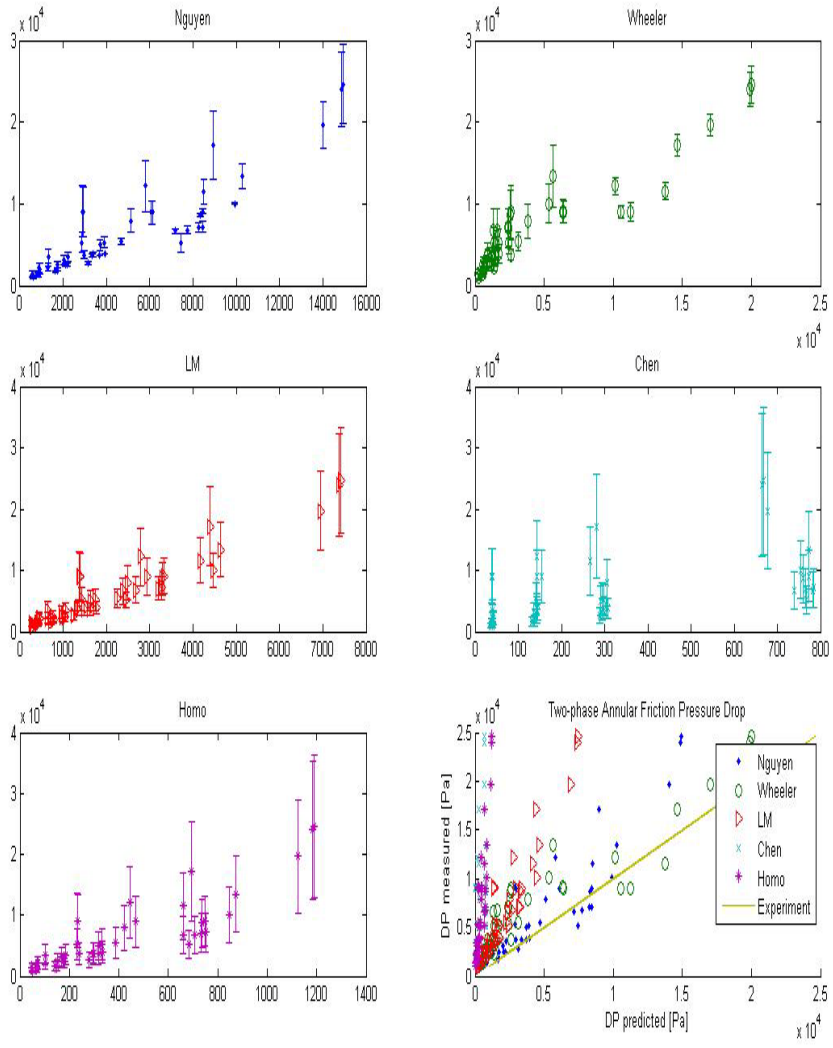

Figure 4.23: Two-phase pressure drop models with error bars (Bousman, 1994)

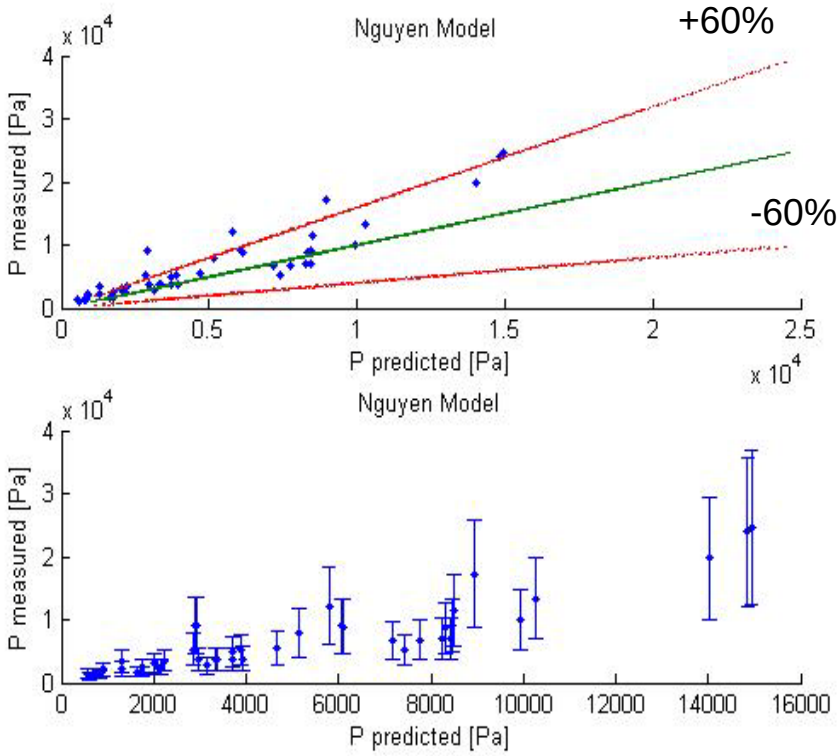

Figure 4.24: Prediction of two-phase pressure drop model on Bousman data

The results shown in Figures 4.22, 4.23 and 4.24 indicate that the new model predicts the measured pressure drops more accurately compared with other models. The homogeneous model completely fails to predict the measured data. Most of the data are not predicted well by Chen model. This can be expected in that the density of R-144 vapor at the condition is 30 times that of air. The gas phase therefore possesses considerably more momentum relative to liquid phase in R-144 system than in the air-water system. This may lead to rupture the liquid slugs to form annular flow at much lower values of superficial gas velocity which means larger pressure drop is expected in Bousman flight data.

4.5.4 Zhao and Rezkallah flight data, 1994 (85 points)

Table 4.7: ΔP average error from Rezkallah

Model	DP average error (%)
New model (2009)	**-88.1941**
LM (1949)	-28.4298
Wheeler (1992)	-48.7542
Chen (1989)	-121.8509
Homogeneous	-122.2039

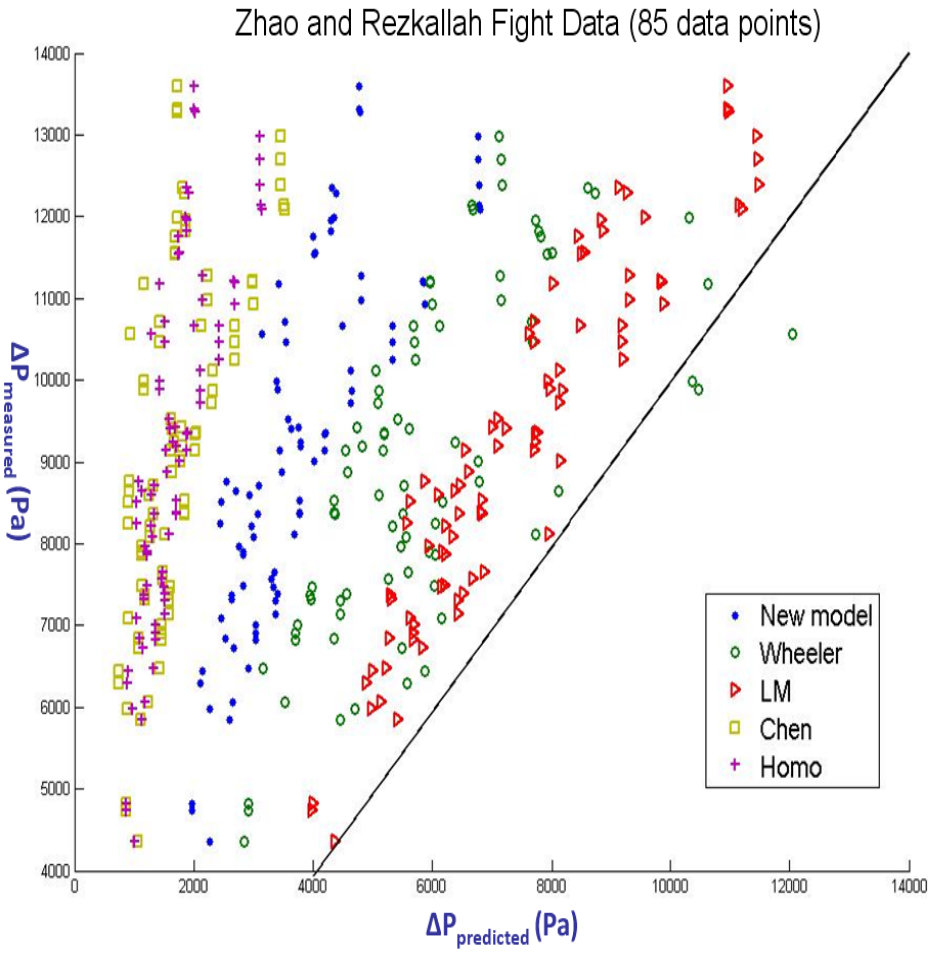

Figure 4.25: Two-phase pressure drop models under 0-g (Rezkallah, 1994)

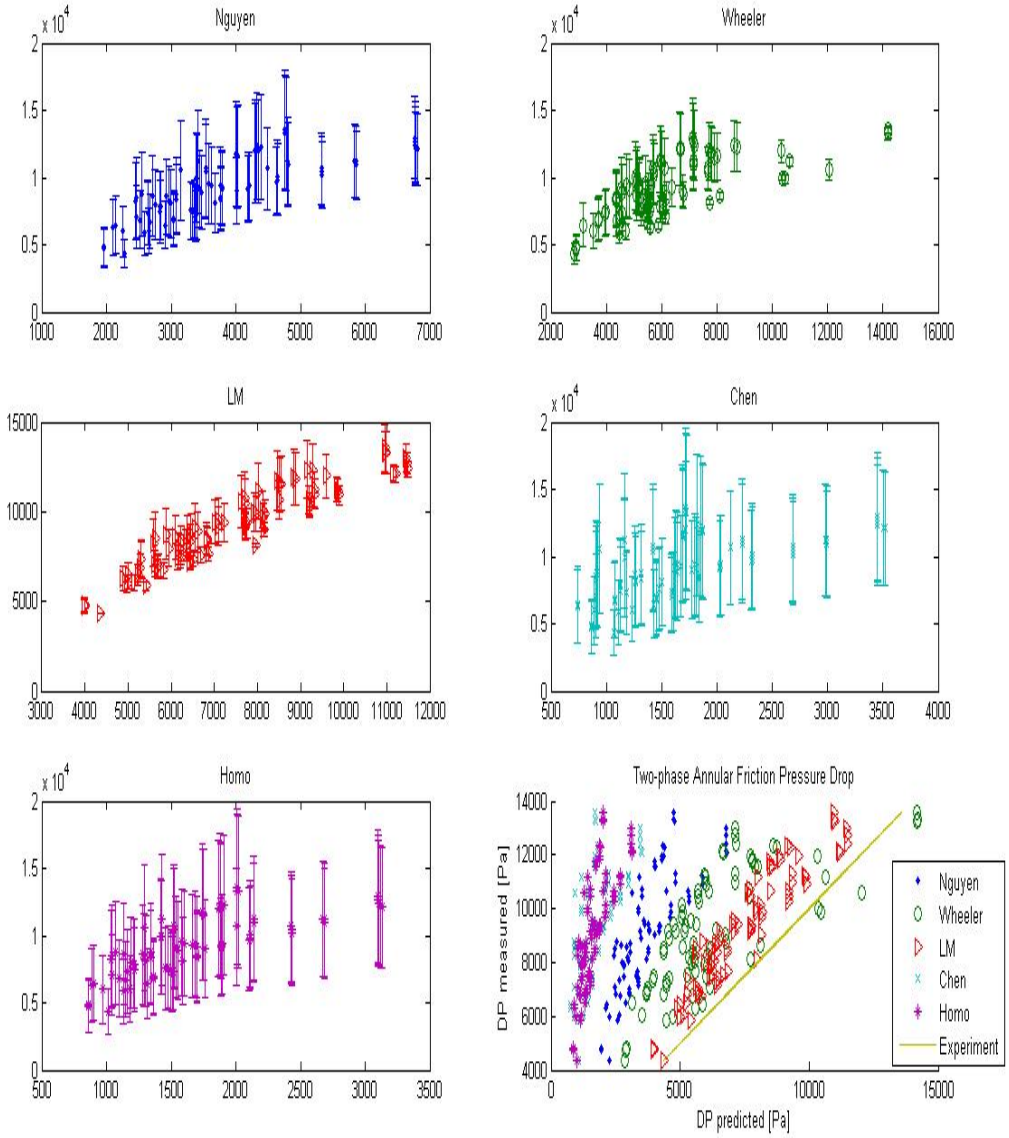

Figure 4.26: Two-phase pressure drop models with error bars (Rezkallah, 1994)

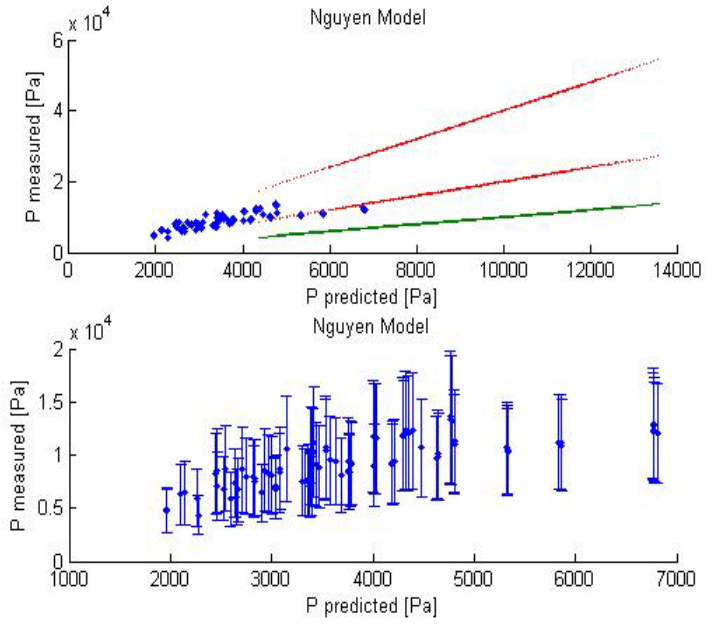

Figure 4.27: Prediction of two-phase pressure drop model on Rezkallah data

Figures 4.25, 4.26 and 4.27 and Table 4.7 show that all models under-predicted the two-phase frictional pressure drop from Zhao and Rezkallah flight data. As seen in Figures 4.15, the annular flow regime in the Rezkallah experiment presented a very high vapor superficial velocity compared with other superficial velocities. Since the two-phase pressure drop is proportional to the square of vapor superficial velocity, leading larger pressure drops in Zhao and Rezkallah flight data. In addition, with such a high vapor superficial velocity, the annular flow regime in our experiment would shift to a mist annular flow regime where no liquid film presents along the tube. Furthermore, entrainment of liquid flow is likely to happen at a very high vapor superficial velocity, and this violates the assumptions of the new model.

4.6 CHAPTER SUMMARY

The results of the film thickness, void fraction and interfacial friction factor modeling were presented. Empirical correlations for the interfacial friction factor and void fraction were developed from 57 points using a linear least squares regression technique. The new pressure drop model can be applied requiring only knowledge of the length and diameter of the tube, liquid and vapor mass flow rates and properties of the working fluid. The new pressure drop model is the optimal model for predicting the two-phase friction pressure drop compared with the Lockhart-Martinelli model, Wheeler model, Chen model and homogeneous model. The new model can predict the two-phase friction pressure drop in annular regimes with the majority of the data fall within +-20% of the proposed correlation and an error of 12 %.

CHAPTER V

SUMMARY AND CONCLUSIONS

5.1 SUMMARY

This thesis presents an experimental and theoretical study of the flow characteristic of annular flow under microgravity conditions. The film thickness, void fraction and frictional pressure drop for R-12 have been examined under microgravity. Microgravity data were collected on board a parabolic aircraft by the Interphase Transport Phenomena (ITP) group from Texas A&M University. Non-dimensional equations were developed to predict the interfacial friction factor and the void fraction by using linear least squares regression technique. The interfacial friction factor and the void fraction were correlated from 57 points with a least square error of 0.0015 and 0.0087 respectively. The frictional pressure drop can be predicted within +- 20% for microgravity by using the new model. Furthermore, the validation and reliability of the new pressure drop were tested using Foster-Miller & ITP data, Sundstrand, and Zhao and Rezkallah data.

5.2 CONCLUSIONS

The following conclusions can be made based on the present work.

1. The film thickness increases with increasing liquid flow rate or decreasing gas flow rate under microgravity. The average film thickness and the height of fluctuations become distinctly larger with decreasing the vapor flow rate.
2. The frictional pressure drop increases by increasing the liquid or gas flow rates under microgravity.
3. There are two mechanisms that drive the liquid velocity under microgravity:
    a. First, without the influence of gravity, the liquid film is subjected to no body forces, and therefore has a higher average velocity than normal gravity. Based on the conversation of mass, a higher velocity causes a decrease in the flow area, which means a thinner mean film thickness.
    b. Second, the liquid movement is effected mostly by the momentum of the vapor. In the annular regime under microgravity, the vapor velocity is much smaller than that at normal gravity; therefore it has a smaller average velocity. Again, based on the conservation of mass, a smaller velocity causes an increase in the flow area, which means a thicker mean film.

   A thicker film was observed in our experiment; therefore the second mechanism seems to dominate the film thickness for annular flow under microgravity.
4. The interfacial friction factor increased linearly with increasing film thickness, which means the interface vapor and liquid surface becomes rougher, and therefore the

pressure drop increases. Since the thicker film was observed, the pressure drop under microgravity was expected larger than that at normal gravity.

5. Compared with the Lockhart-Martinelli model, Wheeler model, Chen model and homogeneous model, the new model accurately predicted two-phase pressure drop from ITP & Creare flight data, Foster-Miller & ITP flight data, and Sundstrand flight data with the lowest average error.
6. Lockhart-Martinelli overpredicts all values of measured pressure drop in all previous 0-g experiments except Zhao and Rezkallah Flight.
7. The new model under-predicted the two-phase frictional pressure drop from Zhao and Rezkallah flight data. The annular flow regime in the Rezkallah experiment presented a very high vapor superficial velocity compared with our experimental superficial velocity. With such a high vapor superficial velocity, the annular flow regime in our experiment would shift to a mist annular flow regime where no liquid film presents along the tube. Furthermore, entrainment of liquid flow is likely to happen at a very high vapor superficial velocity, and this violates the assumptions of the new model.
8. The Wheeler model is the second most accurate model to predict the two-phase pressure drop under microgravity. The annular Flow Model /Chen model can surprisingly predicted our experimental pressure drop with 20% average error. Although Lockhart-Martinelli correlation is simple, it almost fails to predict the two-phase pressure drop under microgravity collected from ITP & Creare flight data, Foster-Miller & ITP flight data and Sundstrand flight data.

5.3 RECOMMENDATIONS

Based on the results and conclusions of this study, the following suggestions for future research can be made:

1. Although the droplet entrainment and deposition was not observed in this study, but the need for direct measurement of entrainment rate is essential in developing a more mechanistic understanding of microgravity annular flows.
2. The pressure drop is strongly affected by the film thickness and the interphase surface between liquid and vapor. Thus, wave characteristics must be studied for a better understanding of annular frictional pressure drop under microgravity.
3. As seen in Figure 4.15, using R-12 shows that large changes occur in the flow regime map with the large changes in the density of the fluids and other physical property changes. The same experiment need to be conducted with many different working fluids such as steam-water, ammonia and others for a better design and operation of two-phase flow systems under microgravity.
4. The new pressure drop model is only valid for a straight tube. For a better performance of the two-phase system, the model should be developed so that it can account for the geometry of the test section (e.g. bends, tees and ect)
5. The amount of microgravity annular flow data is still limited. Further data should be collected to verify the current work.

REFERENCES

[1]W.S. Hill & F.R. Best, "Microgravity Two-Phase Flow Experiment and Test Results", 21st *International Conference on Environmental Systems*, San Francisco, CA, July 15-18, 1991.

[2]I. Chen, R. Downing, E.G. Keshock, & M. Al-Sharif, "*Measurements and Correlation of Two-phase Pressure Drop under Microgravity Condition*", J. Thermo Physics, 1991.

[3] I. Chen, R. Downing, E.G. Keshock, & M. Al-Sharif, "Experimental Study and Prediction of a Two-Phase Pressure Drop in Microgravity", AIAA 27th , Aerospace Sciences Meeting, Reno, Nevada, 1989.

[4]K.S. Gabriel, *Microgravity two-phase flow and heat transfer*, Microcosm Press, El Segundo, CA, 2006.

[5]J.A.Albers and R.P.Macosko, "Condensing Pressure Drop of Nonwetting Mercury in a Uniform Tapered Tube in 1-g and Zero-Gravity Environments", NASA-TN-D-3185,1966.

[6]D.B.Heppner, C.D. King, J.W. Littles, "Zero-G Experiments in Two-Phase Fluids Flow Regimes ", Marshall Space Flight Center, 75-ENAS-24,1975.

[7]M. Wheeler, "An Experimental and Analytical Study of Annular Two-Phase Flow Friction Pressure Drop in a Reduced Acceleration Field", Masters Thesis, Texas A&M University, College Station, Texas, 1992.

[8]A. Lambert, "KC-135 Zero Gravity Two Phase Flow Pressure Drop Experiments and Modeling", Masters Thesis, Texas A&M University, College Station, Texas, 1990.

[9]A. Lambert, T.R. Reinarts, F. Best & W. Hill, KC-135 Zero Gravity Two Phase Flow Pressure Drop Experiments and Modeling, *Proc. of the 8th Symposium on Space Nuclear Power Systems*, Albuquerque, NM, Jan. 6-10, 1991.

[10]E. Miller, E. Ungar, J. Dzenitis & M. Wheeler, "Microgravity Two-Phase Pressure Drop Data in Smooth Tubing", ASME Winter Annual Meeting, New Orleans, LA, 1993.

[11]K. Marsden, C. Kurwitz, F. Best, "*Two-phase Zero-gravity Pressure Drop Prediction from Single-Phase One-g Data*", Journal of Thermophysics and Heat Transfer, Vol. 19, No. 4, 2005.

[12]L. Zhao & K. Rezkallah, "Pressure Drop in Two-Phase Annular Flow at Microgravity Conditions", 31st Aerospace Sciences Meeting & Exhibit, Jan 11-14, 1993, Reno, NV, AIAA 93-0572, 1993.

[13]K. Rezkallah, "*Recent Progress in the Studies of Two-Phase Flow at Microgravity Conditions*", Microgravity Research Group, Adv. Space Res, Vol 16, No. 17,1995.

[14]K.M. Hurlbert, "*Flow Dynamics for Two-Phase Flows in Partial Gravities*", PhD dissertation, University of Houston, Houston, Texas, 2000.

[15]T.R. Reinarts, "*Adiabatic Two Phase Flow Regimes Data and Modeling for Zero and Reduced (Horizontal Flow) Acceleration Fields*", PhD dissertation, Texas A&M University, College Station, Texas,1991.

[16]L. Valota, "Microgravity flow pattern identification using void fraction signals", Masters Thesis, Texas A&M University, College Station, Texas, 2004.

[17]C. Crowley & W. Chen, "Scaling of Multiphase Flow Regimes and Interfacial Behavior at Microgravity", Final Report, Presented to NASA Glenn Research Center, 2001.

[18]V. Georgevich, "Analytical Modeling and Experimental Investigation of Interfacial Waves in Annular Microgravity Two-Phase Flow", PhD dissertation, Texas A&M University, College Station, Texas, 1991.

[19]T. Fukano and T. Furukawa, "*Prediction of the Effects of Liquid Viscosity on Interfacial Shear Stress and Frictional Pressure Drop in Vertical Upward Gas-liquid Annular Flow*", Int. J. Multiphase Flow, Vol. 24, No. 4, 1998, pp. 587-603.

[20]P. de Jong, "A Preliminary Study of Two-phase Annular Flow at Microgravity: Experimental Data of Film Thickness", Int. J. Multiphase Flow, Vol. 29, 2003, pp. 1203-1220.

[21]D. Hill & R. Downhill, "A Study of Two-Phase Flow in a Reduced Gravity Environment", Final Report, Sundstrand Energy Systems, Rockford, IL, 1987.

[22]M. MacGillivray, "Gravity and Gas Density Effects on Annular Flow Average Film Thickness and Frictional Pressure Drop", Masters Thesis, University of Saskatchewan, 2004.

[23]S. Wongwises and W. Kongkiatwanitch, "*Interfacial Friction Factor in Vertical Upward Gas-Liquid Annular Two-Phase Flow*", Heat Mass Transfer, Vol. 28, pp. 323-336, 2001.

[24]V.P. Carey, *Liquid-Vapor Phase Change Phenomena*, Taylor & Francis Group, Berkeley,CA, 2008.

[25]J.G. Collier, *Convective Boiling and Condensation*, Mc Graw-Hill Book Company, New York, 1972.

[26]G.B. Wallis, *One-Dimensional Two-Phase Flow*, McGraw-Hill Book Company, New York, 1969.

[27]K.A. Triplett, S.M. Ghiaasiaan, S.I. Abdel-Khalik, A. LeMouel, B.N. McCord, "*Gas-Liquid Two-phase flow in Microchannels Part II: Void Fraction and Pressure Drop*", International Journal of Multiphase Flow 25, 1999.

[28]E.K. Ungar, "Single Phase vs. Two-Phase Active Thermal Control Systems for Space Applications: a Trade Study", NASA-Johnson Space Center,1995, paper #AIAA-95-0634.

[29]R.Balasubramaniam, E.Rame, J. Kizito, and M.Kassemi, "Two Phase Flow Modeling: Summary of Flow Regimes and Pressure Drop Correlations in Reduced and Partial Gravity", National Center for Space Exploration Research, Cleveland, OH, 2006.

APPENDIX A

ITP & Creare Flight Data (2000)

Test ID	$\delta_{3mm, up}$ (mm)	$\alpha_{135mm, up}$ (-)	$mdot_f$ (g/s)	$mdot_g$ (g/s)	j_f (m/s)	j_g (m/s)	$\Delta P_{corrected}$ (Pa)	g_z (g)	Regime
20222	0.96	0.67	49.66	7.29	0.293	1.948	2066	0.03	A
20221	0.96	0.67	49.59	7.23	0.293	1.932	2033	0.02	A
20223	1.06	0.64	50.06	6.13	0.296	1.64	1681	0.02	A
20225	1.47	0.52	50.94	2.69	0.301	0.719	909	0.02	A
20208	0.59	0.78	33.19	12.69	0.196	3.392	3142	0.01	A
20209	0.65	0.76	33.43	10.62	0.198	2.838	2533	0.02	A
20210	0.72	0.73	33.74	8.62	0.199	2.304	1968	0.02	A
20211	0.85	0.7	33.91	6.38	0.2	1.706	1410	0.01	A
20212	1	0.66	34	4.54	0.201	1.214	986	0.02	A
20213	1.22	0.57	34.37	2.89	0.203	0.772	630	0.04	A
20214	1.41	0.54	34.11	2.1	0.201	0.56	479	0.02	A
20207	0.55	0.79	24.9	10.01	0.147	2.677	2131	0	A
13020	0.61	0.76	25.03	8.14	0.148	2.176	1520	0.03	A
1306	0.77	0.71	25.4	5.63	0.15	1.506	909	0.04	A
13019	0.75	0.72	24.93	5.58	0.147	1.492	960	0.02	A
20205	0.82	0.71	24.88	4.5	0.147	1.203	851	0.01	A
13018	1.05	0.63	25.4	2.93	0.15	0.782	439	0.03	A
20206	1.21	0.59	25.47	2.38	0.15	0.636	370	0.01	A
20188	0.39	0.84	16.13	13.84	0.095	3.699	2252	0.02	A
20187	0.45	0.82	16.21	10.4	0.096	2.781	1574	0.02	A
20186	0.51	0.8	16.3	8.38	0.096	2.24	1220	0.02	A
20185	0.58	0.77	16.19	6.27	0.096	1.677	808	0.01	A
20183	0.72	0.73	16.66	4.41	0.098	1.18	542	0.02	A
20184	0.72	0.73	16.45	4.34	0.097	1.161	471	0	A
20182	0.88	0.68	16.41	3	0.097	0.803	341	0.01	A
20181	0.88	0.69	16.67	2.98	0.098	0.796	308	0.01	A
20180	1.07	0.62	16.19	1.98	0.096	0.529	163	0.01	A
13161	0.28	0.89	10.41	13.23	0.061	3.538	1850	0.03	A
20189	0.39	0.85	11.16	10.02	0.066	2.678	1187	0.03	A
20190	0.42	0.83	11.15	8.34	0.066	2.23	931	0.02	A
13011	0.54	0.79	10.31	4.18	0.061	1.117	383	0.03	A
1305	0.69	0.73	10.28	3.15	0.061	0.841	155	0.04	A
13012	0.69	0.74	11.03	3.01	0.065	0.805	232	0.02	A
13013	0.84	0.7	10.88	2.02	0.064	0.539	136	0.03	A
20168	0.24	0.92	7.46	13.96	0.044	3.732	1708	0.01	A
20169	0.27	0.9	7.53	10.09	0.044	2.697	1035	0.03	A

20170	0.3	0.89	7.79	8.58	0.046	2.294	807	0	A
20171	0.39	0.85	7.82	6.21	0.046	1.661	561	0	A
20172	0.46	0.82	8	4.42	0.047	1.183	318	0	A
20173	0.6	0.78	8.36	3.09	0.049	0.827	147	0	A
20174	0.75	0.73	7.76	2.02	0.046	0.54	100	0.01	A
20175	0.97	0.65	8.42	1.01	0.05	0.27	26	0.01	A
20176	1.14	0.62	8.58	0.99	0.051	0.265	30	0.01	A
13139	0.15	0.95	4.65	13.87	0.027	3.707	1193	0.02	A
13140	0.17	0.95	4.46	10.7	0.026	2.861	728	0.01	A
13141	0.19	0.94	4.48	8.83	0.026	2.359	555	0.02	A
13142	0.25	0.91	4.63	6.43	0.027	1.718	334	0.01	A
13143	0.32	0.88	4.7	4.53	0.028	1.212	221	0.03	A
13146	0.41	0.85	4.87	3.06	0.029	0.818	62	0.02	A
13147	0.53	0.79	5.41	2.05	0.032	0.548	49	0.02	A
13148	0.81	0.67	5.43	0.99	0.032	0.265	6	0.02	A
13160	0.09	0.96	1.94	13.82	0.011	3.695	659	0.03	A
13159	0.14	0.94	1.89	10.67	0.011	2.853	491	0.03	A
13158	0.16	0.94	1.99	8.83	0.012	2.36	348	0.03	A
13157	0.25	0.91	1.88	3.01	0.011	0.805	13	0.02	A
13156	0.24	0.91	2.2	2.92	0.013	0.781	71	0.02	A
13153	0.34	0.88	1.92	2.06	0.011	0.551	33	0	A
13155	0.28	0.89	1.8	1.97	0.011	0.527	73	0.02	A
13152	0.54	0.81	1.94	1.02	0.011	0.272	59	0.01	A
13150	0.62	0.73	1.71	0.26	0.01	0.07	4	0.02	A

ITP & Foster-Miller/ Wheeler Flight Data (1992)

Temp (K)	System Pressure (kPa)	Total mass flow rate (kg/s)	Quality	Corrected pressure drop (section 1) (kPa)	Corrected pressure drop (section 2) (kPa)	Flow regime
290.4	533.5	0.00715	0.641	0.397	0.385	AN
290.2	531.0	0.00720	0.632	0.423	0.361	AN
289.8	525.9	0.00740	0.614	0.495	0.381	AN
290.2	529.3	0.00852	0.525	0.416	0.377	AN
290.1	526.7	0.00858	0.530	0.398	0.387	AN
290.2	528.3	0.00862	0.527	0.372	0.363	AN
289.1	516.5	0.00893	0.399	0.578	0.467	AN
288.6	508.4	0.00909	0.408	0.582	0.421	AN
288.8	514.0	0.00915	0.401	0.581	0.373	AN
289.6	518.8	0.01030	0.384	0.504	0.424	na
288.7	504.0	0.01112	0.396	0.654	0.587	AN
288.9	507.9	0.01118	0.390	0.657	0.592	AN
288.9	506.7	0.01120	0.396	0.628	0.603	AN
291.7	515.7	0.01125	0.884	0.601	0.648	AN
290.3	514.2	0.01132	0.873	0.590	0.682	AN
290.0	524.3	0.01143	0.532	0.833	0.804	AN
290.2	526.9	0.01145	0.536	0.811	0.782	AN
291.5	515.0	0.01146	0.863	0.585	0.738	AN
290.0	522.7	0.01146	0.534	0.824	0.798	AN
288.3	497.6	0.01175	0.705	0.993	0.890	AN
293.2	506.0	0.01177	0.942	0.616	0.835	AN
292.3	505.1	0.01182	0.934	0.635	0.816	AN
293.2	507.1	0.01191	0.933	0.589	0.874	AN
289.9	503.8	0.01225	0.899	1.575	1.476	na
288.8	502.9	0.01227	0.856	1.832	1.555	AN
288.7	501.4	0.01230	0.849	1.886	1.599	AN
289.2	505.5	0.01235	0.862	1.697	1.430	AN
289.5	503.4	0.01236	0.895	1.607	1.422	na
290.0	508.8	0.01237	0.903	1.595	1.457	na
288.2	495.7	0.01362	0.455	0.918	0.826	na
289.6	510.7	0.01395	0.820	2.293	1.989	AN
289.4	511.5	0.01398	0.823	2.059	2.036	AN
289.6	513.2	0.01409	0.825	2.073	1.937	AN
289.1	512.3	0.01449	0.332	1.401	1.291	AN
288.3	496.7	0.01455	0.425	0.909	0.838	na
289.7	520.1	0.01472	0.331	1.394	1.268	AN
289.2	515.4	0.01476	0.329	1.365	1.200	AN

288.2	493.7	0.01476	0.535	1.520	1.446	AN
288.4	496.9	0.01486	0.537	1.523	1.448	AN
290.7	537.6	0.01520	0.115	0.332	0.257	AN/SL
290.3	530.3	0.01592	0.108	0.308	0.278	AN/SL
288.9	508.9	0.01595	0.319	1.651	1.462	AN
289.1	510.8	0.01607	0.318	1.658	1.513	AN
288.7	505.3	0.01610	0.316	1.669	1.505	AN
288.4	494.0	0.01623	0.622	1.882	1.844	AN
288.5	497.2	0.01658	0.619	1.891	1.759	AN
289.4	510.0	0.01662	0.614	2.093	2.050	AN
289.4	509.5	0.01688	0.619	2.061	2.032	AN
288.6	497.7	0.01690	0.613	1.833	1.748	AN
290.8	532.6	0.01716	0.280	1.020	0.992	AN
290.5	528.3	0.01722	0.278	1.027	1.010	AN
290.8	535.2	0.01726	0.280	1.012	0.973	AN
289.5	518.9	0.01978	0.170	1.225	1.080	AN
289.0	514.6	0.01981	0.169	1.212	1.058	AN
288.7	506.7	0.01983	0.165	1.301	1.107	AN
292.3	561.5	0.01999	0.072	0.299	0.287	SL/AN
292.2	559.1	0.02023	0.070	0.293	0.287	SL/AN
292.1	556.9	0.02038	0.064	0.254	0.284	SL/AN
289.4	516.6	0.02122	0.100	0.560	0.456	AN/SL
289.6	518.5	0.02128	0.116	0.578	0.613	AN/SL
289.7	519.0	0.02141	0.116	0.581	0.623	AN/SL
289.2	514.2	0.02168	0.098	0.517	0.531	AN/SL
289.6	518.4	0.02172	0.114	0.596	0.606	AN/SL
289.4	507.4	0.02214	0.413	2.605	2.736	na
288.8	498.4	0.02217	0.382	2.425	2.429	AN
289.4	508.6	0.02234	0.408	2.592	2.723	na
289.1	502.8	0.02236	0.385	2.418	2.450	AN
289.0	500.9	0.02237	0.386	2.396	2.429	AN
290.7	531.2	0.02427	0.177	1.232	1.273	AN/FR
291.0	534.8	0.02447	0.180	1.247	1.254	AN/FR
290.9	533.3	0.02463	0.176	1.239	1.257	AN/FR
289.1	503.1	0.03618	0.164	3.705	3.797	AN
288.9	502.8	0.03622	0.166	3.805	3.649	AN
289.8	516.4	0.04389	0.049	1.175	1.303	AN/FR
289.9	518.0	0.04391	0.050	1.203	1.331	AN/FR
289.9	518.6	0.04401	0.049	1.299	1.333	AN/FR
290.4	521.4	0.04806	0.100	4.003	3.958	AN
291.0	532.5	0.04857	0.102	3.787	3.831	AN
290.2	523.5	0.04947	0.100	3.606	3.517	AN
291.8	544.5	0.05964	0.049	1.827	1.938	AN/FR
292.1	549.5	0.06052	0.048	1.835	1.916	AN/FR
292.1	549.4	0.06063	0.048	1.817	1.899	AN/FR

APPENDIX B

PRESSURE DROP CODES

```
clear; clc; close all;

%**************Read database******************

fileName = 'cal.xls';
a = xlsread(fileName);

%**************Test geometry******************
Pi = 3.14;
D = 12.7*10^-3;                     %Diameter [m]
L = 163*10^-2;                      %Length [m]
A = Pi*D^2/4;                       %Cross section Area [m^2]

%****************R-12*****************************

pf = 1320;                          %liquid density [kg/m^3]
pg = 34;                            %vapor density [kg/m^3]
muf = 2.3*10^-4;                    %liquid viscosity [Pa-s]
mug = 1.2*10^-5;                    %vapor viscosity [Pa-s]
sigma = 0.01;

%**************Measured void fraction and film thickness*********

voidup135 = a(:,2);
filmup3 = 10^-3*a(:,10);                % film thickness [m]
film = filmup3;                         % liquid film from 3mm sensor
[m]
void = voidup135;                       % void fraction from 135mm
sensor
dfilm = film/D;                         % Dimensionless film thickness

%************Basic Parameters************************************

Pexpt = a(:,13);                     % Measured pressure drop [Pa]
mf = 10^-3*a(:,8);                   % liquid mass flow rate [kg/s]
mg = 10^-3*a(:,9);                   % vapor mass flow rate [kg/s]
G = (mf + mg)/A;                     % mass flux [kg/m2-s]
x = mg./(mg+mf);                     % mass quality
jg = G.*x./pg;                       % vapor superficial velocity [m/s]
jf = G.*(1-x)./pf;                   % liquid superficial velocity [m/s]
ug = mg./(pg*A.*void);               % vapor velocity [m/s]
uf = mf./(pf*A.*(1-void));           % liquid velocity [m/s]
Ref = G.*(1-x)*D/muf;                % liquid Reynolds number
Reg = G.*x*D/mug;                    % vapor Reynolds number
```

```
mu_2phases = (x./mug + (1-x)./muf).^-1;  %two-phase viscosity

%*******************Interfacial friction factor
correlation***************

fw = 0.079*(G*D./mu_2phases).^(-1/4);           % Blasius equation
fi_expt= 1/2*Pexpt./(pg*jg.^2./void.^2.5)*D/L;   % fi correlated by the
measured pressure drop
fmodel = 0.005*(1+50.6807*dfilm).^0.8796;         % fmodel with error
0.0015
figure (75)
fmodel1 = 0.32*dfilm + 0.0072;
er_fi = (fi_expt - fmodel1).^1/2;
errorbar(fmodel1,fi_expt,er_fi,'.');

%***********************Void fraction*********************************

X= (1-x)./x;
P= pg/pf;
M= muf/mug;

Voidmodel = 1./(1 + 1.1809*(X).^0.646.*(P).^1.2135.*(M).^0.7989);
%vmodel with error 0.0087
er_void = (Voidmodel - void).^1/2;
figure (80)
errorbar(Voidmodel,void,er_void,'.');

%***********************Premoli void*********************************

beta = jg./(jg+jf);
y = beta./(1-beta);
Re = G*D/muf;
We = G.^2*D./(sigma*pf);
E1 = 1.578*Re.^-0.19*(pf/pg)^0.22;
E2 = 0.0273*We.*Re.^-0.51*(pf/pg)^-0.08;
S = 1 + E1.*(y./(1+y.*E2)- y.*E2).^(1/2);
void_Pre = (x/pg)./(x/pg + S.*(1-x)/pg);

%***********************other voids*********************************'

Xtt = P.^0.5*M.^0.125*X.^0.875;         %Martinelli parameter

n1=[1 ; 1    ; 0.72 ; 0.64 ; 1    ; 0.74 ];
n2=[1 ; 0.67 ; 0.40 ; 0.36 ; 0.89 ; 0.65 ];
n3=[0 ; 0    ; 0.08 ; 0.07 ; 0.18 ; 0.13 ];
BB=[1 ; 1    ; 1    ; 0.28 ; 1    ; 1    ];

void_homo=     (1+BB(1)*X.^n1(1)*P^n2(1)*M^n3(1)).^(-1);   %homogeneous
model
void_Zivi=     (1+BB(2)*X.^n1(2)*P^n2(2)*M^n3(2)).^(-1);   %Zivi model
```

```
void_Wallis =  (1+BB(3)*X.^n1(3)*P^n2(3)*M^n3(3)).^(-1);   %Wallis
separate cylinder model
void_LM =      (1+BB(4)*X.^n1(4)*P^n2(4)*M^n3(4)).^(-1);   %Lockhart
and Martinelli
void_Thom =    (1+BB(5)*X.^n1(5)*P^n2(5)*M^n3(5)).^(-1);   %Thom
correlation
void_Baroczy = (1+BB(6)*X.^n1(6)*P^n2(6)*M^n3(6)).^(-1);   %Baroczy
correlation

%***********************other interfacial friction
factor*********************************'
fi_Wallis = 0.005*(1 + 300*dfilm);
fi_Moeck = 0.005*(1 + 1458*dfilm.^1.42);
fi_Chen = 0.005*(1 + 11.7*dfilm.^0.39);

%********************** Nguyen Model
*********************************


fi_Nguyen =fmodel;
void_Nguyen = Voidmodel;
P_Nguyen = 2*(L/D)*fi_Nguyen.*(pg*jg.^2./void_Nguyen.^2.5);
figure(3);
hold on
xlabel('P predicted [Pa]');
ylabel('P measured [Pa]');
title ('Nguyen Model');
plot(P_Nguyen,Pexpt,'.',Pexpt,Pexpt,'-
',Pexpt,1.8*Pexpt,'r:',Pexpt,1.1*Pexpt,'r:')
text (P_Nguyen(1),Pexpt(5),'%80')
text (P_Nguyen(2),Pexpt(7),'%10')
hold off

%***********************L-M Model*******************************

fi_LM = 0.005*(1+75.*(1-void_LM));                          % Wallis
P_LM = 2*L/D*fi_LM.*(pg*jg.^2./void_LM.^2.5);
figure(4);
hold on
xlabel('P predicted [Pa]');
ylabel('P measured [Pa]');
title ('LM Model');
text (P_LM(1),Pexpt(6),'-%40')
text (P_LM(1),Pexpt(7),'-%50')
plot(P_LM,Pexpt,'.',Pexpt,Pexpt,'-
',Pexpt,0.5*Pexpt,'r:',Pexpt,0.6*Pexpt,'r:')
hold off


%***********************Wheeler Model*******************************

mu_TP = 1./(x/mug + (1-x)./muf);
Re_TP = D*G./mu_TP;
```

```
void_Wheeler = (1 - 6.476*Xtt.^0.4935.*Re_TP.^-0.3535).^2;
S_Wheeler = ((1-void_Wheeler)./void_Wheeler).*(pf/pg).*(x./(1-x));
fi_Wheeler = 0.0032 + 0.076*void_Wheeler.^(1/2)*(pf/pg).*S_Wheeler.^-
2.*Ref.^-0.25;
P_Wheeler = 2*L/D*fi_Wheeler.*(pg*jg.^2./void_Wheeler.^2.5);
figure(5);
hold on
xlabel('P predicted [Pa]');
ylabel('P measured [Pa]');
title ('Wheeler Model');
text (P_Wheeler(1),Pexpt(5),'%10')
text (P_Wheeler(2),Pexpt(7),'-%35')
plot(P_Wheeler,Pexpt,'.',Pexpt,Pexpt,'-
',Pexpt,1.1*Pexpt,'r:',Pexpt,0.65*Pexpt,'r:')
hold off


%**********************Chen Model**********************************

void_Chen = void;
P_Chen = 2*L/D*fi_Chen.*(pg*jg.^2./void_Chen.^2.5);
figure(7);
hold on
xlabel('P predicted [Pa]');
ylabel('P measured [Pa]');
title ('Chen Model');
text (P_Chen(1),Pexpt(5),'30%')
text (P_Chen(2),Pexpt(30),'-40%')
plot(P_Chen,Pexpt,'.',Pexpt,Pexpt,'-
',Pexpt,1.3*Pexpt,'r:',Pexpt,0.6*Pexpt,'r:')
hold off

%**********************Homogeneous
Model*****************************

fi_homo = 0.005*(1+75.*(1-void_homo));                          % Wallis
P_homo = 2*L/D*fi_homo.*(pg*jg.^2./void_homo.^2.5);
figure(12);
hold on
xlabel('P predicted [Pa]');
ylabel('P measured [Pa]');
title ('Homo Model');
text (P_homo(2),Pexpt(5),'50%')
text (P_homo(1),Pexpt(7),'-%20')
plot(P_homo,Pexpt,'.',Pexpt,Pexpt,'-
',Pexpt,0.8*Pexpt,'r:',Pexpt,1.5*Pexpt,'r:')
hold off

%**************************Figure**************************************
***8
figure(8);
hold on
```

```
xlabel('DP predicted [Pa]');
ylabel('DP measured [Pa]');
title ('Two-phase Annular Friction Pressure Drop');
plot(P_Nguyen,Pexpt,'.',P_Wheeler,Pexpt,'o',P_LM,Pexpt,'>',P_Chen,Pexpt
,'x',P_homo,Pexpt,'*')
legend('New model','Wheeler','LM','Chen','Homo');
hold off
figure(10);
hold on
plot(void_Nguyen,void,'.',void_Wheeler,void,'o',void_Wallis,void,'x',vo
id_LM,void,'>',void_Baroczy,void,'*',void_Thom,void,'+',void_homo,void,
'square',void_Zivi,void,'<');
legend('New
void','Wheeler','Wallis','LM','Baroczy','Thom','Homo','Zivi');
hold off
figure(11);
hold on
plot(fmodel1,fi_expt,'.',fi_Wallis,fi_expt,'+',fi_Chen,fi_expt,'*',fi_W
heeler,fi_expt,'o');
legend('New void','Wallis','Chen','Wheeler')
hold off

%**********************************film*****************************
*****************
film_model = 0.23*(1-void)-0.0035;
figure (90)
plot(dfilm,1-void,'.',film_model,1-void,'o');

%************************error in
void**********************************
evoid_Nguyen = sum((void_Nguyen - void)./void)/57;
stdvoid_Nguyen = (1/57*sum(void_Nguyen - evoid_Nguyen)^2)^(1/2);

evoid_Wheeler = sum((void_Wheeler - void)./void)/57;
stdvoid_Wheeler = (1/57*sum(void_Wheeler - evoid_Wheeler)^2)^(1/2);

evoid_Wallis = sum((void_Wallis - void)./void)/57;
stdvoid_Wallis = (1/57*sum(void_Wallis - evoid_Wallis)^2)^(1/2);

evoid_LM = sum((void_LM - void)./void)/57;
stdvoid_LM = (1/57*sum(void_LM - evoid_LM)^2)^(1/2);

evoid_Baroczy = sum((void_Baroczy - void)./void)/57;
stdvoid_Baroczy = (1/57*sum(void_Baroczy - evoid_Baroczy)^2)^(1/2);

evoid_Thom = sum((void_Thom - void)./void)/57;
stdvoid_Thom = (1/57*sum(void_Thom - evoid_Thom)^2)^(1/2);

evoid_homo = sum((void_homo - void)./void)/57;
stdvoid_homo = (1/57*sum(void_homo - evoid_homo)^2)^(1/2);

evoid_Zivi = sum((void_Zivi - void)./void)/57;
```

```
stdvoid_Zivi = (1/57*sum(void_Zivi - evoid_Zivi)^2)^(1/2);

evoid = 100*[evoid_Nguyen;
evoid_Wheeler;evoid_Wallis;evoid_LM;evoid_Baroczy;evoid_Thom;evoid_homo
;evoid_Zivi];
stdvoid = [stdvoid_Nguyen;
stdvoid_Wheeler;stdvoid_Wallis;stdvoid_LM;stdvoid_Baroczy;stdvoid_Thom;
stdvoid_homo;stdvoid_Zivi];

%**********************error in fi*****************************

efi_Nguyen = sum((fi_Nguyen - fi_expt)./fi_expt)/57;
stdfi_Nguyen = (1/57*sum(fi_Nguyen - efi_Nguyen)^2)^(1/2);

efi_Wallis = sum((fi_Wallis - fi_expt)./fi_expt)/57;
stdfi_Wallis = (1/57*sum(fi_Wallis - efi_Wallis)^2)^(1/2);

efi_Chen = sum((fi_Chen - fi_expt)./fi_expt)/57;
stdfi_Chen = (1/57*sum(fi_Chen - efi_Chen)^2)^(1/2);

efi_Moeck = sum((fi_Moeck - fi_expt)./fi_expt)/57;
stdfi_Moeck = (1/57*sum(fi_Moeck - efi_Moeck)^2)^(1/2);


efi_Wheeler = sum((fi_Wheeler - fi_expt)./fi_expt)/57;
stdfi_Wheeler = (1/57*sum(fi_Wheeler - efi_Wheeler)^2)^(1/2);

efi = 100*[efi_Nguyen; efi_Wallis;efi_Chen;efi_Moeck;efi_Wheeler];
stdfi =[stdfi_Nguyen;
stdfi_Wallis;stdfi_Chen;stdfi_Moeck;stdfi_Wheeler];

%**********************error in
P***************************************
error_Nguyen = sum((P_Nguyen - Pexpt)./Pexpt)/57;
er_Nguyen = (P_Nguyen - Pexpt).^1/2;
std_Nguyen = (1/57*sum(P_Nguyen1 - error_Nguyen1)^2)^(1/2);

error_LM = sum((P_LM - Pexpt)./Pexpt)/57;
std_LM = (1/57*sum(P_LM - error_LM)^2)^(1/2);
er_LM = (P_LM - Pexpt).^1/2;

error_Wheeler = sum((P_Wheeler - Pexpt)./Pexpt)/57;
std_Wheeler = (1/57*sum(P_Wheeler - error_Wheeler)^2)^(1/2);
er_Wheeler = (P_Wheeler - Pexpt).^1/2;

error_Chen = sum((P_Chen - Pexpt)./Pexpt)/57;
std_Chen = (1/57*sum(P_Chen - error_Chen)^2)^(1/2);
er_Chen = (P_Chen - Pexpt).^1/2;

error_homo = sum((P_homo - Pexpt)./Pexpt)/57;
std_homo = (1/57*sum(P_homo - error_homo)^2)^(1/2);
```

```
er_homo = (P_homo - Pexpt).^1/2;

errorP = 100*[error_Nguyen;
error_LM;error_Wheeler;error_Chen;error_homo];
stdP = [std_Nguyen; std_LM;std_Wheeler;std_Chen;std_homo];
%*********************************************************************
figure (9)

subplot(3,2,1);
title ('Nguyen Model');
errorbar(P_Nguyen,Pexpt,er_Nguyen1,'.');

subplot(3,2,2);
title ('Wheeler Model');
errorbar(P_Wheeler,Pexpt,er_Wheeler,'o');

subplot(3,2,3)
title ('LM Model');
errorbar(P_LM,Pexpt,er_LM,'>');

subplot(3,2,4);
title ('Chen Model');
errorbar(P_Chen,Pexpt,er_Chen,'x');

subplot(3,2,5);
title ('Homo Model');
errorbar(P_homo,Pexpt,er_homo,'*');

subplot(3,2,6);
hold on
xlabel('DP predicted [Pa]');
ylabel('DP measured [Pa]');
title ('Two-phase Annular Friction Pressure Drop');
plot(P_Nguyen1,Pexpt,'.',P_Wheeler,Pexpt,'o',P_LM,Pexpt,'>',P_Chen,Pexp
t,'x',P_homo,Pexpt,'*',Pexpt,Pexpt,'-')
legend('Nguyen','Wheeler','LM','Chen','Homo','Experiment');
hold off

%*********************************************************************
*
figure (30)
subplot(3,2,1);
hold on
xlabel('DP predicted [Pa]');
ylabel('DP measured [Pa]');
title ('Nguyen Model ');
text (P_Nguyen(1),Pexpt(5),'20%')
text (P_Nguyen(2),Pexpt(7),'-20%')
plot(P_Nguyen1,Pexpt,'.',Pexpt,Pexpt,'-
',Pexpt,1.2*Pexpt,'r:',Pexpt,0.8*Pexpt,'r:');
hold off
```

```
subplot(3,2,2);
hold on
xlabel('DP predicted [Pa]');
ylabel('DP measured [Pa]');
title ('Wheeler Model');
text (P_Wheeler(1),Pexpt(5),'10%')
text (P_Wheeler(2),Pexpt(7),'-%35')
plot(P_Wheeler,Pexpt,'.',Pexpt,Pexpt,'-
',Pexpt,1.1*Pexpt,'r:',Pexpt,0.65*Pexpt,'r:')
hold off

subplot(3,2,3)
hold on
xlabel('DP predicted [Pa]');
ylabel('DP measured [Pa]');
title ('LM Model');
text (P_LM(1),Pexpt(6),'-40%')
text (P_LM(1),Pexpt(7),'-50%')
plot(P_LM,Pexpt,'.',Pexpt,Pexpt,'-
',Pexpt,0.5*Pexpt,'r:',Pexpt,0.6*Pexpt,'r:')
hold off

subplot(3,2,4);
hold on
xlabel('DP predicted [Pa]');
ylabel('DP measured [Pa]');
title ('Chen Model');
text (P_Chen(1),Pexpt(5),'30%')
text (P_Chen(2),Pexpt(30),'-40%')
plot(P_Chen,Pexpt,'.',Pexpt,Pexpt,'-
',Pexpt,1.3*Pexpt,'r:',Pexpt,0.6*Pexpt,'r:')
hold off

subplot(3,2,5);
hold on
xlabel('DP predicted [Pa]');
ylabel('DP measured [Pa]');
title ('Homo Model');
text (P_homo(2),Pexpt(5),'50%')
text (P_homo(1),Pexpt(7),'-20%')
plot(P_homo,Pexpt,'.',Pexpt,Pexpt,'-
',Pexpt,0.8*Pexpt,'r:',Pexpt,1.5*Pexpt,'r:')
hold off

%************************************************
figure (32)
hold on
plot(Xtt,void_Nguyen,'.',Xtt,void,'o');
legend('New void','Measured void');
hold off

figure (33)
subplot(2,1,1);
```

```
hold on
xlabel('P predicted [Pa]');
ylabel('P measured [Pa]');
title ('Nguyen Model ');
text (P_Nguyen(1),Pexpt(5),'%20')
text (P_Nguyen(2),Pexpt(7),'-%20')
plot(P_Nguyen1,Pexpt,'.',Pexpt,Pexpt,'-
',Pexpt,1.2*Pexpt,'r:',Pexpt,0.8*Pexpt,'r:');
hold off
subplot(2,1,2);
hold on
xlabel('P predicted [Pa]');
ylabel('P measured [Pa]');
title ('Nguyen Model ');
title ('Nguyen Model');
errorbar(P_Nguyen,Pexpt,er_Nguyen,'.');
hold on
figure(27)
plot(1-void,dfilm,'.')
figure(28)
errorbar(P_Nguyen,Pexpt,er_Nguyen,'.');
```

FLOW REGIMES CODES

```
clear; clc; close all;

%**************Read database*****************

fileName = 'flowRegime.xls';
a = xlsread(fileName);
jg_Nguyen = a(:,1);
jf_Nguyen = a(:,2);
jg_Chen = a(:,3);
jf_Chen = a(:,4);
jg_Wheeler = a(:,5);
jf_Wheeler = a(:,6);
jg_Kah = a(:,7);
jf_Kah = a(:,8);
jg_Bou = a(:,9);
jf_Bou = a(:,10);

liquid_density = [1320;100;1466];
vapor_density = [34;1;14.3];
liquid_viscosity = [2.3*10^-4;1*10^-5;2.36*10^-4];
vapor_viscosity = [1.2*10^-5;1.2*10^-5;1.56*10^-5];
surface_tension = [0.01;0.07;0];
figure(1)
hold on
xlabel('jg [m/s]');
ylabel('jf [m/s]');
title ('Annular Flow Regime');
plot(jg_Nguyen,jf_Nguyen,'.',jg_Chen,jf_Chen,'o',jg_Wheeler,jf_Wheeler,
'x',jg_Kah,jf_Kah,'>',jg_Bou,jf_Bou,'+');
legend('ITP&Creare','Chen','Wheeler','Kezkallah','Bousman');
hold off
figure(2)
hold on
xlabel('pg*jg^2 [kg/s2-m]');
ylabel('pf*jf^2 [kg/s2-m]');
title ('Annular Flow Regime');
plot(vapor_density(1)*jg_Nguyen.^2,liquid_density(1)*jf_Nguyen.^2,'.',v
apor_density(3)*jg_Chen.^2,liquid_density(3)*jf_Chen.^2,'o',vapor_densi
ty(1)*jg_Wheeler.^2,liquid_density(1)*jf_Wheeler.^2,'x',vapor_density(2
)*jg_Kah.^2,liquid_density(2)*jf_Kah.^2,'>',vapor_density(2)*jg_Bou.^2,
liquid_density(2)*jf_Bou.^2,'>');
legend('Nguyen','Chen','Wheeler','Kezkallah','Bousman');
hold off
```

LEAST SQUARES METHOD

```
function error = file(p)
fileName = 'film.xls';
a = xlsread(fileName);
fi_expt = a(:,1);
dfilm = a(:,2);
Fmodel = 0.005*(1+p(1)*dfilm.^p(2));
error = sum((fi_expt - Fmodel).^2);


function error = findvoid(p)
fileName = 'film.xls';
a = xlsread(fileName);
void = a(:,3);
X = a(:,4);
P = a(:,5);
M = a(:,6);
Fmodel = 1./(1 + p(1)*(X).^p(2).*(P).^p(3).*(M).^p(4));
error = sum((void - Fmodel).^2);


function error = xvoid(p)
fileName = 'film.xls';
a = xlsread(fileName);
void = a(:,3);
Xtt = a(:,7);
Fmodel = 1./(1 + p(1)*(Xtt).^p(2));
error = sum((void - Fmodel).^2);
```

VITA

Ngoc Thanh Nguyen was born in Saigon, Vietnam. He attended Le Hong Phong high school for the gifted and graduated in May 2001. He received his Bachelor of Science degree in nuclear engineering from Texas A&M University in December 2007. He remained at Texas A&M University to pursue his graduate studies in the Nuclear Engineering Department. He received his M.S. degree in December 2009. He can be reached at:

Department of Nuclear Engineering
Texas A&M University
3133 TAMU
College Station, TX 77843-3133.